1984

Final report on i-470 wheeling bridge hanger cables and cracks in tie girder diaphragms, 1984

J. W. Fisher

A. W. Pense

R. G. Slutter

C. C. Menzemer

FINAL REPORT ON I470 WHEELING BRIDGE HANGER CABLES AND CRACKS IN TIE GIRDER DIAPHRAGMS

by

John W. Fisher

Alan W. Pense

Roger G. Slutter

Craig C. Menzemer

Eric J. Kaufmann

for the

West Virginia Department of Highways

Fritz Engineering Laboratory

Lehigh University

Bethlehem, Pennsylvania

November 1984

Fritz Engineering Laboratory Report No. 491.1(84)

TABLE OF CONTENTS

I. INTRODUCTION

Cracked wires discovered at the cable hanger connection to the tie girders of the I470 bridge at Wheeling, West Virginia were verified to be caused by fatigue. This resulted from fretting of the outer wires in the cable against steel shims at the end fittings.[3]

This study was in part carried out to assess the significance of the cracking on the residual fatigue and static strength of damaged and undamaged cables.

In order to assess the significance of the cracked wires found in the hanger cables, extensive tests were carried out on cables removed from the structure. This included cables with cracked wires and some with no detectable damage. The studies included fatigue tests of the 2-1/4 in. cables, dissection of several cable sockets to evaluate the interior wires, and tensile tests on the cables.

During the course of the studies cracks were detected in the tie girders at diaphragms where floor beams framed into the tie girders. Several segments of these cracked elements were removed from the diaphragms so that fractographic studies could be carried out on the crack surfaces.

In order to establish the causes of the cracking in the diaphragm-web welded connections, strain measurements were initially acquired with controlled loads. It was thought that some evidence of wind induced cyclic stress would be observed during those studies, but none was observed during the week the measurements were acquired. The results of the controlled load studies are evaluated and reported herein.

Subsequently, measurements were acquired on a few gages by installing the recording equipment so that measurements could be obtained at pre-selected wind velocities. This provided response records at wind velocities of 25, 30, 35, and 40 mph. These results are also evaluated and reported.

II. STUDIES ON THE BRIDGE HANGER CABLES

1. Fatigue Tests of 2-1/4 in. Strand

Six full sections removed from the bridge structure were fabricated into test specimens, as illustrated in Fig. 1. Three of the specimens had broken wires. New swaged end fittings were attached to one end of the test specimen in order to grip the specimen in the alternating stress machine. Figure 2 shows a specimen mounted in the test machine and under cyclic load.

The first specimen selected (Spec. F) for testing was from the center section of hanger 8SE and had no detectable damage. The cyclic loads for this specimen were selected using a minimum stress level equal to the average dead load stress and the maximum stress equal to the sum of the average dead and live load stress. This resulted in a cyclic stress range of 7 ksi and a minimum stress of 43 ksi. More than 5 million cyclic loads were applied to the test specimen without any detectable damage.

The results of all the cyclic cable tests are summarized in Table 1. Since no fatigue cracking was detected after the first tests, the next two specimens were tested at a cyclic stress of about 10 ksi or 43% greater than the first cyclic test. These specimens were identified as Specimens D and E. Specimen E was from location 8SE and had no detectable broken wires. It was subjected to 3.83 million cycles without any detectable damage. The second specimen D was from the bottom of cable 8SE and had three broken wires. It was subjected to 4.19 million cycles without any damage developing in the remaining wires of the cable.

The other two specimens tested were subjected to a cyclic stress of 14 ksi. This is 100% greater than the average design live load stress. The specimens were identified as Specimens B and C. Specimen C was from the bottom end of 5'NW and Specimen from 7NW. Only Specimen B had broken wires prior to testing. It was subjected to 4.79 million cycles without any evidence of distress. Specimen C was subjected to 4.84 million cycles and also showed no evidence of distress.

The cyclic tests have verified that the suspender cables have suffered no significant damage as a result of the wind induced vibration that caused fretting fatigue in several of the hanger cables. This resulted from the fretting of the cable against the steel keeper plates. Only those cable wires that were rubbed against the steel keepers sustained damage. Four of the five tests have been carried out at cyclic stress levels well in excess of the average design load condition and have experienced no adverse affects.

2. Dissection of Cables Adjacent to Sockets

Several cable ends were supplied in their button sockets so that the individual wires could be examined in the outer and inner layers to ascertain whether or not any additional fatigue damage could be found. Figure 3 shows a schematic of the pieces that were supplied for this purpose. The socket was removed from the end of Specimens G, H, and I by first saw cutting the socket and prying the wires from the cut segments. Figure 4 shows the saw cut socket and part of the remaining wires.

The outer layer of wires could be removed from the splayed ends that were embedded in the zinc that had been poured into the socket without great difficulty. Great difficulty was experienced in separating the wires from the interior layers.

2.1 Dissection of Three 3 ft. Lengths Adjacent to Sockets

Dissection and examination of Samples G, H, and I was carried out as follows. The sockets were removed from the cables and the individual wires were separated for examination. These examinations showed no incidence of wire breakage within the interior wire (second and third layers) and no evidence of associated gouge or groove marks on the interior wires. All fractures had occurred in outside wires.

2.2 Examination of Broken Wires

Broken wires were examined from Specimens I; H, and D. In every instance, these wires were found in the outside layers and the fractures were associated with gouges or rub marks on the wires. The broken wires

were examined using scanning electron microscopy (SEM). In this process the fracture surface is scanned with a beam of electrons and back-scattered electrons are collected and displayed on a CRT. By using suitable scanning techniques, this allows much higher resolution and depth of field than the light microscope, although the images produced appear to be like light microscope views.

Typical results of these studies are shown in Figs. 5 to 18. As shown in Figs. 5 to 7, visual examination of a broken wire from Sample I shows a slightly slant fracture with some rub marks just visible on the surface of the wire at the lowest level of the slant. Figure 7 shows a gouge mark on the wire surface at the fracture location. The end view of this wire is seen in Fig. 8. The corroded condition of the fracture surfaces of these wires is clearly seen in Fig. 8.

Scanning electron microscopy of broken wire I-1 from Specimen 1 produced the result seen in Fig. 9. Here the wire surface is seen to be covered with a corrosion layer, and surface features are not particularly evident. Because all of the wires appeared to be in this condition, a cleaning solution developed at Lehigh was applied[(2)]. This solution has been shown to effectively remove oxide coatings, and for short treatment times, leaves the underlying fracture features unchanged. The same wire, after cleaning treatment, is shown in Fig. 10.

It is now evident that failure of this wire was by a fatigue mechanism, as may be seen from the "beach marks" on the crack surface. The initiation point on the wire is at the right-hand side of Fig. 10, which corresponds to a rub or gouge mark. The final fracture was the steep

slant fracture region on the left. The overall load on the wire was not high, as fatigue cracking progressed through at least 50% of the wire cross-section before fracture occurred.

A second broken wire, from Specimen H, wire H-1, is seen in Fig. 11 and as cleaned and examined by SEM in Fig. 12. The fatigue "beach marks" on this surface are more faint because of the more extensive cleaning required, and this attacks the fracture surface as well as the corrosion layer. However, an initiation point at a surface gouge is seen at the lower left position of the crack surface. The final fracture region is to the upper right.

SEM examination of three additional broken wires taken from Specimen D, wires D-1, D-2, and D-3, produced the results seen in Figs. 13 to 18. These figures show clearly that the mechanism of failure is by fatigue in every case, with slant failure being produced as a final stage after cracking was extensive. In each case, some corrosion product was left on the surface, which produces, in some instances, a dark spot on the image due to electron charging effects in the SEM. Complete removal of all oxide was not desirable, as the "beach marks" would also be partially removed in the process. In each case a gouge mark accompanied crack initiation.

It is therefore apparent that all broken wires are caused by fatigue initiating at surface rub marks, and all failed wires are on outside layers. These cracked wires appear identical to those examined in 1981 from the same structure[3].

3. Tensile Strength of Cable 7NW

The lower end of hanger 7NW had no broken wires and was fabricated into a tensile specimen with 15 ft. between the sockets, as shown in Fig. 19. The existing button socket was retained, and a new open socket was added. The specimen was mounted in the 5,000,000 lb. testing machine and initially loaded in 25 kip increments from 50 kips to 280 kips. Elongation measurements were obtained over a 100 in. length in order to determine the elastic modulus of the strand. Thereafter, the load was increased in 50 kip increments until 550 kips was reached, and then at 10 kip increments until 640 kips was reached. Five kip increments were added until failure at 664 kips.

The load strain response is plotted in Fig. 20. The elastic modulus between the 50 kip and 280 kip load levels was calculated to be 26,900 ksi.

The original socketed cable end was observed to have pulled out about 5/8 in. after the test as the zinc anchorage seated. All of the wire breaks exhibited a cup-cone shape indicative of a ductile failure mode. The ultimate capacity was well in excess of minimum expected failure capacity of 620 kips. The cable showed no adverse affect from its prior service and aeroelastic vibration. Whatever fretting may have been experienced had not initiated any micro-cracking in any wire.

4. Tensile Tests on Individual Wires

Four lengths of the individual wires removed from Specimen G as it was taken apart were individually tested to establish the tensile characteristics of the wire. The results of these tests are summarized in Table 2. All wires were observed to satisfy the minimum 0.7% strain yield point of 160 ksi. The yield strength varied from 171 to 189 ksi. The tensile strength varied from 229 ksi to 236 ksi which was in excess of the minimum tensile strength of 220 ksi required by ASTM A586.

The elongation varied between 6.33 and 8.5% which was well in excess of the minimum 4% elongation.

5. Tensile Tests on Fatigue Tested Cables

Three of the 70 in. long fatigue test specimens that had new swaged fittings installed on the cut end were tested to failure. Figure 21 shows a photograph of Specimen E after it was subjected to nearly 4 million cycles of stress range equal to 10 ksi.

Two of the three specimens were tested to failure in the 800 kip testing machine. Specimens A, D, and E were selected for these tensile strength tests. Specimen A had not been subjected to cyclic stress and provided a reference condition. Both Specimens D and E were subjected to about 10 ksi nominal stress range at the estimated dead load condition.

Specimen D had been supplied with three broken wires, whereas Specimens A and E had no detectable broken wires before and after the fatigue tests.

All three of the specimens failed at the swaged fitting, as can be seen in Fig. 22. None of the wires broke at the original button sockets.

Table 3 provides a summary of the test results. Specimen A with no broken wires and not fatigue tested provided about the same capacity as Specimen E with no broken wires but subjected to 4 million stress cycles. The maximum load was 573 kips for Specimen A and 578.5 kips for Specimen E. Specimen D with three broken wires failed at 520.5 kips.

All of the test results are below the catalog ultimate strength of the strand. This resulted because the swaged fitting is not adequate to develop the ultimate strength of the cable. The fitting selected was the largest swaged fitting that would fit into the head of the alternating stress testing machine. This controlled the selection and no attempt was made to select a fitting that would develop the cable capacity. The attempt to develop the cable capacity by extending the wires through the fitting did not succeed.

Nevertheless, the test results clearly demonstrate that no significant damage was sustained by any of the remaining wires at the original button sockets. No damage was detected during the fatigue tests, and none of the wires failed during the ultimate load tests. The reduced capacity of the specimens was solely caused by the use of swaged fittings and the nonuniform distribution of load in the wires at these fittings.

III. STUDIES OF FLOOR BEAM DIAPHRAGM - WEB WELD CRACKING

1. Fractograph Study of Segments Removed from Tie Girders

Six samples were removed from the tied arch box tie girder diaphragms for fractographic analysis. These include samples from panel points 6, 6', and 3' in the north tie and panel points 8, 3', and 4' in the south tie. Each of the samples was examined for evidence of cracking, and an assessment made as to whether or not sufficient fracture surface was available to perform scanning and/or Transmission Electron Microscopy on these samples. Based on this assessment, fractographic examination was undertaken of samples 3'S, 4'S, and 6NW, while general study including macroetching of weld areas was undertaken on the remaining samples. Since all these samples are similar, only representative ones are cited in this report.

1.1 General Appearance of Segment Samples

The segment samples removed from the structure are seen in Figs. 23 to 28, as received. As may be seen, samples taken near the end of the diaphragm, for example 6N, 4'N and 3'S, have an additional piece produced by the crack surface between the girder box web and the diaphragm. When the core was removed, the additional pad also separated or was removed by grinding. For many cases, the grinding damaged part of the crack surface, although some was usually left for examination. A number of small pieces, with some crack surface present, are seen in Figs. 26, 27, and 28. It is also evident from examinations of the diaphragm end samples that the fillet

welds between the diaphragm end samples did not always extend down to the diaphragm end, leaving an unfused, or partially fused condition at this location. This is particularly evident in Fig. 23. Careful examination of this sample showed that, in addition to a short second fillet weld pass, there was a significant region of slag inclusion under the second pass, leaving an unfused fillet weld leg of length of about 0.75 in. from the diaphram end. Several other samples showed similar, although less severe, unfused regions.

1.2 Etched Sections

Several of the specimens were polished and etched to examine the cracking extending from the roots of the partial penetration fillet welds in the diaphram to web attachment. These samples are seen in Figs. 29 to 31. As these samples show, the lack of penetration region in the fillet weld connection is variable. However, its true size is difficult to estimate in a sample cut in this manner. The gap shown in Fig. 30 is probably most typical. Cracking is seen in all three of these etched sections, as indicated by the arrows. In most cases, the crack passes through the weld metal. Although in one case, sample 4's (see Fig. 30), cracking results in a slight heat affected zone lamellar tear. An apparent crack is seen in the weld metal of samples 3'S which is not indicated by an arrow (see Fig. 29). This is actually an interpass lack of fusion region, not a crack.

1.3 Fractographic Studies

The fracture surface area of several samples were examined for evidence of the nature of the fracture process involved. The results of these studies are seen in Figs. 32 to 39. Scanning electron micrographs of portions of sample 4'S (see Figs. 32 to 34) showed evidence of fatigue crack growth and ductile tearing. The evidence of fatigue crack growth is most clear in Figs. 32 and 33, with broad striations clearly shown in Fig. 32, and striations mixed with ductile tearing seen in Fig. 33. Figure 34 shows evidence of ductile tearing. The mixed nature of the fracture surface suggests that crack growth proceeded at very high levels of stress range (high stress intensity range, ΔK). Both the broad striations and dimple rupture are characteristics of high stress range fatigue. Scanning electron micrographs from sample 6N also showed ductile tearing, as seen in Fig. 35.

Transmission electron micrographs were prepared from replicas taken from sample 3'S. Here the fatigue striations are clearly seen in Fig. 36 and 37, and dimple rupture can be seen in Figs. 38 and 39. Once again this suggests that the fatigue crack growth developed at high ΔK levels. From the striation spacing in Figs. 36 and 37, it appears that the crack growth rates are between 0.6 and 1.4 x 10^{-5} in/cycle for this sample.

2. Strain Measurements with Controlled Loads

2.1 Instrumentation

In order to assess the cracking that developed in the floor beam diaphragm weld to web connections, strain gages were mounted at panel points 4' and 8 in the north tie girder. Altogether, 35 strain gages were mounted between the two panel points*. Panel point 4' had four strain gages mounted on the diaphragm and a total of twelve gages mounted in three web gaps, as shown in Fig. 40. Panel point 8 had seven diaphragm gages and a total of twelve gages mounted in three web gaps, as illustrated in Fig. 41. Panel point 4' was monitored because a 3/8 in. long crack existed at the bottom of the east weld, while panel point 8 was monitored because no detectable cracking was apparent.

It was hoped that strain measurements could be acquired during a period of moderate to high wind velocity. But, during the measurement period between September 9 through September 13, 1983, no weather patterns developed that resulted in high winds. Structural response was obtained from two loaded test trucks on September 9, 1983. Each truck had five axles and was loaded to a total gross weight of 80 kips.

A total of eighteen test runs were carried out with the two test trucks. Nine runs were westbound and nine runs were eastbound. Six of the runs had the vehicles traveling side by side, and the remaining twelve runs had the vehicles traveling one behind the other.

---

*All of the field instrumentation and measurements were carried out by Messrs. Harry Laatz and K. Nelson of the Turner Fairbanks Highway Research Center of the Federal Highway Administration.

2.2 Test Results

In general, the strain measurement - time records show that a large response occurs as the vehicles cross the floor beam at the gaged locations, as can be seen in Figs. 42 and 43. This response is characteristic of both the web gap regions and the diaphragm. In addition, the records also show that each truck produced one major stress cycle. It is also evident that all gages showed some degree of stress reversal.

From the strain measurement records, gradients in the web gaps at the maximum and minimum response during the stress cycle were constructed. Typical gradients are provided in Figs. 44 to 52. The difference between the two gradients represents the stress range. The results indicate that most of the web gaps are distorted in double curvature in the gap. This indicates that the web is being displaced out-of-plane relative to the flange. Lack of stiffness in the web gap due to the partial depth diaphragm is the primary reason for the high cyclic stresses.

Several displacement shapes were drawn that corresponded to the measured stress. Two distinct times were chosen from the strain measurement records. The distortions in the gaps were drawn qualitatively that corresponded to the measured gradients. Figures 53 and 54 show these relatively deformed shapes for two time intervals. The measurements and displaced shapes indicate that the floor beam end restraint moment is reversed, as would be expected from the deformed shapes shown schematically in Fig. 55. To evaluate the out-of-plane bending, the stress gradients were extrapolated to the end of the diaphram welds and to the bottom of the backing bar. Table 4 gives a summary of the estimated stress ranges

at each of the four web gaps at panel points 4' and 8. At the bottom flange, the backup bar was not fillet welded to the web and flange. At the top flange, the backup bar was fillet welded to the web and flange.

The largest stress ranges were observed to occur at the bottom inside web gap at panel point 4' (floor beam side, see Fig. 52). A summary of the stress ranges observed during the eighteen test runs at gage B11 is given in Table 5. These gage measurements show that the largest stress ranges were observed when the trucks were traveling abreast. In addition, eastbound runs produced larger stress range values than the corresponding westbound runs. Truck speed had a negligible influence on the observed stress ranges.

Table 5 also summarizes the stress range values for gage B8 which is located at the outside bottom gap of panel point 4'. While the stress ranges are lower than those observed at B11, the values are in the range of 2.5 to 5 ksi. As was the case with gage B11, the largest stress ranges were observed when the trucks were traveling abreast. Again, eastbound runs produced larger stress range values than westbound runs. Velocity had a negligible influence on the stress ranges.

Table 5 also provides the stress range values for gages B4 and A4. These gages are located in the upper outside web gap near the diaphragm at panel point 4' and 8. The stress range values are of the order 1.0 - 2.5 ksi for gage B4.

The largest stress range values at panel point 8 occurred in the upper outside gap at gage A4. The results are also summarized in Table 5. The

results at panel point 8 were comparable to the results observed at panel point 4'. Larger stress ranges were observed with the trucks traveling abreast. Truck speed had negligible influence. Test runs in the westbound direction gave stress ranges higher than corresponding eastbound runs.

Stress ranges occurring at gages A8 and A11 were small (0.5 - 1.7 ksi). But in both cases, westbound runs produced higher stress ranges than eastbound runs. Again, speed had little influence, and the highest stress ranges were observed with the trucks traveling abreast.

2.3 Analysis of Test Results

A comparison of the test results for panel points 4' and 8 show some major differences. Generally, trucks traveling eastbound produced larger responses at panel point 4' than trucks traveling westbound. However, trucks traveling westbound produced a larger response at panel point 8 than trucks traveling eastbound.

The largest stress ranges at panel point 4' were caused by vehicles traveling eastbound or away from the gaged location. The measurements suggest that the gap responses result from the double curvature bending of the floor beam and the relative displacement between the two tie girders, as illustrated in Fig. 55. The double curvature occurs because the floor beam is loaded through the bridge deck and stringers. Bending is also developed due to the relative displacement between the two tie girders. The displacement is due to the truck(s) traveling on one side of the bridge centerline or the other. With the trucks traveling eastbound, the

moment due to double curvature bending and the moment due to relative displacement between tie girders add. Hence, at panel point 4', trucks traveling eastbound produce a larger response than trucks traveling westbound.

The largest stress ranges at panel point 8 are caused by vehicles traveling westbound, or adjacent to the gaged section. The moment introduced into the tie girder diaphragm connection with the trucks traveling adjacent to the gaged section is greater than the moment produced by trucks traveling eastbound.

The largest stress ranges were observed in the web at panel point 4' where cracking was detected in the diaphragm weld. The largest stress ranges were also found in the inside web gap at the floor beam connection. These observed stress ranges are large enough to result in crack growth in the tie girder web from the lack-of-fusion area with the backup bar. This detail provides a relatively severe notch condition for out-of-plane bending. Such cracks will form parallel to the primary stress field from the axial forces and bending in the tie girder. Hence, crack growth will not be detrimental to the structure at this stage.

The strain measurements on the diaphragms demonstrated that significant stress range cycles can develop in the diaphragm normal to the girder web. The magnitude of the stress range was greatest at the upper edge of the diaphragm plate adjacent to the top flange. The diaphragm stress range values are tabulated in Table 6.

The test results are in good agreement with the finite element analysis carried out by Modjeski and Masters[4].

3. Strain Measurements of Wind Induced Response

In order to obtain test data on possible wind induced response of the tie girder, strain gages at panel points 4' and 8 were connected into Vishay amplifiers and a Kyowa seven channel precision cassette recorder. The system was installed in the structure on April 14-15, 1984. All units were connected to a wind scope indicator and the switch was set to a pre-selected wind speed. Initially, the wind velocity critical speed was set at 25 mph. When the velocity was reached the tape recorder was turned on and recorded the strain response for about one and a half hours until the end of the cassette tape.

After a tape was recorded the velocity indicator was set 5 mph higher, and the sequence repeated. This resulted in records of 25, 30, 35, and 40 mph acquired on April 17, May 6, May 21, and July 6, 1984, respectively.

The strain records were scanned with an oscilloscope in order to establish whether or not wind induced response was apparent. For the tapes acquired for the 25 mph setting, no discernable response was observed. Only random truck crossings were obtained, and these were directly comparable to the responses shown in Figs. 42 and 43.

At the higher wind velocities, an aeroelastic response was observed. Figures 56 and 57 show the response observed during the first 32 sec. interval when the wind velocity reached 30 mph. At the end of the initial 16 sec. (Fig. 56) interval, an oscillation started to develop that continued on during most of the next 16 sec. period (see Fig. 57). Vehicles crossing the span obviously interferred with the response. The frequency

of oscillation was about 1.5 Hz. The magnitude of the gage responses in Figs. 56 and 57 is about equal to half the response observed during the test runs summarized in Tables 5 and 6.

When the wind gage was set to 35 mph, the response observed during the initial 32 sec. period is shown in Figs. 58 and 59. All three gages show that an oscillation develops after eight seconds that is larger in magnitude, but is dampened shortly after eighteen seconds. It appears that the wind velocity decreased abruptly, although vehicle crossings may have also had an effect. Once again the frequency of oscillation was about 1.5 Hz.

The largest and longest sustained oscillation was observed at 40 mph. The response is shown in Figs. 60 and 61. Not much can be seen to develop during the first 16 sec. shown in Fig. 60. However, thereafter, significant oscillations can be seen with superimposed truck response throughout the next 16 sec. interval (see Fig. 61). The magnitude of the response was comparable to the truck traffic summarized in Table 5.

The results observed in Figs. 56 to 61 indicate that significant cyclic stresses could be developed as the tie girders oscillated. The cyclic stress occurred at a frequency of 1.5 Hz. Hence, each hour of such response would accumulate 5400 stress cycles in the web gap and welded connection.

4. Analysis of Crack Propagation

Near the ends of the diaphragm - outer web bransverse welds, the weld size tends to decrease in size, and some evidence of lack of fusion between the multiple weld passes of the 3/8 in. welds was observed. This lack of fusion together with the unfused thickness of the 1/2 in. diaphragm plate provides a large crack-like defect that is parallel to the primary stresses in the tie girder and hence has no affect on the tie girder. However, as the strain measurements from wind induced oscillation and trucks have demonstrated, a cyclic stress range is developed in the diaphragm, and this cyclic stress is perpendicular to the lack of fusion, as illustrated schematically in Fig. 62.

The stress intensity factor for this lack of fusion condition can be estimated from the equation.

$$\frac{K\left(A_1 + A_2 \frac{a}{w}\right)\sigma\sqrt{\pi a \sec\frac{\pi a}{2w}}}{1 + \frac{2H}{t_p}} \qquad (1)$$

Where $W = H + \frac{t_p}{2}$

$$A_1 = 0.528 + 3.287\left(\frac{H}{t_p}\right) - 4.361\left(\frac{H}{t_p}\right)^2 + 3.696\left(\frac{H}{t_p}\right)^3 - 1.875\left(\frac{H}{t_p}\right)^4 + 0.415\left(\frac{H}{t_p}\right)^5$$

$$A_2 = 0.218 + 2.717\left(\frac{H}{t_p}\right) - 10.171\left(\frac{H}{t_p}\right) + 13.122\left(\frac{H}{t_p}\right)^3 - 7.755\left(\frac{H}{t_p}\right) + 1.783\left(\frac{H}{t_p}\right)^5$$

At the weld ends, the value of H was observed to be 0.13 to 0.25 in. The unfused widths corresponding to the initial crack size, 2a, varied between 0.4 in. and 0.65 in. The larger value resulted from lack of fusion between weld passes which extended the unfused area.

Furthermore, the presence of ductile dimples near the lower end of the diaphragm at panel points 3'S, 4'S, 6N cited in Section III.1 indicates that some crack extension likely occurred during construction as the end plated diaphragm was bolted to the web and floor beam end plate. Significant forces could result and cause the advancement of the lack-of-fusion plane as the crack tip capacity was exceeded. Hence, larger initial crack sizes likely existed at a number of floor beam - diaphragms that attributed to lack of fusion observed. Such crack advancement would not be apparent on the weld surface, as this would represent a root crack which is not detectable from the surface. Any magnetic particle inspection at the time of weld fabrication would not have revealed subsequent crack extensions, even if they were close to the surface.

The crack and geometric conditions shown in Fig. 62 indicate that stress cycles greater than 1.2 ksi will result in fatigue crack growth if Eq. 1 is equated to the crack growth threshold taken as $\Delta K = 2.75$ ksi $\sqrt{\text{in.}}$ for the greatest lack of fusion and smallest weld leg. For the more usual condition of lack of fusion and weld leg the cyclic stress would need to exceed 2.4 ksi to result in crack growth.

The striation spacing observed during the fractographic examination of the sample removed from panel point 3'S indicated that the growth rate varied from 0.6 to 1.4 x 10^{-5} in/cycle. This rate of growth was detected near the lower end of the diaphragm.

If the crack growth is equated to the relationship

$$\frac{da}{dN} = 3.6 \times 10^{-10} \Delta K^3 \qquad (2)$$

stress intensity ranges between 25.5 ksi $\sqrt{in.}$ and 33.9 ksi $\sqrt{in.}$ result. This level of ΔK is compatible with the observed mode of crack growth discussed in Section III.1. It corresponds to a stress range of 10 to 20 ksi.

The results of the fracture surface examination suggests that the stress range that resulted in crack growth was substantially higher than the stress cycles produced by the test trucks during runs 17 and 18 which are summarized in Tables 3 and 4. Those runs produced stress cycles above the crack growth threshold. However, the stress range was between 2 and 3 ksi, which is much lower than the estimated values of 10 to 20 ksi that result from the striation spacing. It seems probable that aeroelastic response resulted in larger stress cycles.

5. Observations in the Web Gap

In order to assess the effects of the web gap bending distortion, several segments of the backup bars were removed from the box corners at the diaphragm.

The web - flange weld fused into a backing bar, as shown schematically in Fig. 63. Web gap bending stresses can result in fatigue crack growth from the weld root (see Fig. 63), and from the lack of fusion between the backing bar and flange.

A comparison of the vertical and horizontal lack of fusion planes several inches away from the diaphragm with the condition directly at the diaphragm suggested that crack extension had occurred at the diaphragm from these lack of fusion planes. Figure 64 shows a photograph of the web gap and the transitioned end of the backing bar on the right side of the print. The liquid penetrant indication under the diaphragm was about 1/4 in. further in than at the backing bar.

At one location, the liquid penetrant provided an indication at the weld toe of the fillet weld used to connect the backing bar to the flange. This can be seen in Fig. 65. The edge of the scale is aligned with the weld toe position. At the ground bottom flange surface indications can be seen along the weld toe.

IV. STUDIES OF CRACKED HANGER SUPPORT ANGLE

1. General Appearance of Sample

The cracked hanger support removed for study is seen in Fig. 66. The cracked section is seen most clearly along the left end of the support along the toe of the fillet weld joining the two legs of the hanger support which actually extends the entire length of the fillet weld. This is seen more clearly in Fig. 67 and Fig. 68 which show the left and right ends of the hanger support fillet weld. The cracked section penetrates through the weld joint in its widest sections, and at the right end of the hanger. Figure 69 shows a region along the outside of the hanger support angle where the crack has penetrated completely through the section.

1.1 Sample Removed for Study

The cracked areas were sectioned in several places to determine the causes for cracking. Sectioning transverse to the fillet weld close to the right end of the angle (Fig. 68) resulted in complete separation of the member into two pieces. The fracture surface so produced was quite corroded and had apparently been in place for a long time. Additional cuts were made through the cracked weld section in several locations where through cracking had not occurred, so that samples for metallographic study could be removed. These samples were given as standard metallographic polishing sequence using SiC and Al_2O_3 abrasives in water. The cracked section was filled with hot wax prior to this process to prevent abrasives from being forced in the crack and to permit subsequent etching

of the polished section without staining of the etched sample. After polishing, the samples were given an etch in 2% nital (2% nitric acid in methyl alcohol) and examined with a light microscope at magnifications up to 1000X.

1.2 Results of Metallographic Examination

The results of this examination are seen in Figs. 70 through 73. Figures 70 and 71 show the overall configuration of the weld joints in the hanger support angle with the location of the cracks indicated. The welds are seen to be multipass full penetration ones, and the cracks are seen to initiate (based on crack width) at the toe of the weld inside the angle and extend initially along the fusion line (but just inside the heat affected zone).

The crack moves from this weld zone to the plate itself (in Figs. 70 and 71, the vertical leg) and extended in a delaminating mode to the heat affected zone of the weld on the outside of the angle. At this location it follows the heat affected zone close to the fusion line until it comes to the irregular fusion zone of one or more final or "cap" passes on the outside weld where it terminates.

1.3 Cracking Causes and Sequence

Examination of the progression of the crack indicates there are two primary modes of cracking present, hydrogen induced delayed cracking and lamellar tearing. Figures 72 and 73 show the crack progression in the samples seen in Figs. 70 and 71 at higher magnification (100X). In each

case the nominal end of the crack is shown, with the weld metal at the (lower) left hand portion of the photographs and the base plate at the right, i.e., about the same orientation as in Figs. 70 and 71. The intergranular nature of some of the crack surface, and the multiple cracking in some locations establishes this primarily as a hydrogen induced delayed or cold crack, although the possibility of some heat affected zone hot cracking as well is not excluded. The linking of the cracks between the two HAZ areas, seen in Figs. 70 and 71, was by lamellar tearing of the plate. From the width of the crack, as mentioned previously, it appears that the crack initiated as a hydrogen induced cold crack right at the weld toe.

This sequence of cracking is perfectly consistent with the A514 material used for the hanger support. This steel requires extra care in perheat to avoid cold cracking, and this is frequently not taken seriously enough by fabricators. Moreover, some of the cracks apparently appear after considerable time has passed, and this could be missed in inspections. The lamellar tearing in this steel is also not surprising, as the inclusion content of the plate is high (Fig. 73), and the welding residual stress pattern (and joint design) is one that promotes lamellar tearing.

That both of these forms of cracking occur together is also not unusual, as research at Lehigh on lamellar tearing[5] has shown hydrogen will increase the tendency for tearing in some steels. In this case, it provided an initiating crack (a cold crack) for the tear to grow from as well.

1.4 Time of Cracking Formation

The question of the sequence of cracking, i.e., before, during, or after fabrication of the structure is difficult to establish by metallography alone, but is clearly established by the opening of the fracture surface by cutting of the weld. At several points along the weld toe proposed as the initiation site, the blue paint on the plate surfaces has extended into the crack surface, which can only mean that some of this cracking was present during fabrication of the structure. This painted region is seen in Fig. 74. It is also possible that some of the areas of cracking had not extended to the weld surfaces until after completion of construction.

1.5 Fatigue Crack Extension

On the basis of the metallographic examination and fracture surface observation, the major portions of the crack was present, although possibly not all was open to the surface, prior to or during the fabrication of the bridge. It is interesting to note that there is some evidence for a small amount of fatigue crack extension from the top of one of the cracked regions. This is seen in Fig. 75 as a small thin hair-like crack growing from the larger rounded crack. Although it is anticipated that crack growth by fatigue in this location may be limited, given the size of the crack, some extension is likely. As can be seen from Fig. 75, however, this is quite limited, about two or three mils.

V. SUMMARY AND CONCLUSIONS

1. Hanger Cables

(a) The wind induced vibrations of the bridge hanger cables that resulted in fretting induced cracks of several wires did not adversely affect the fatigue resistance nor ultimate capacity of the cables.

(b) Fatigue tests of cables with and without broken wires demonstrated that 4-5 million cycles of twice the design live load could be sustained without any evidence of distress. Ultimate load tests after the fatigue tests demonstrated that none of the wires had any evidence of fatigue damage.

(c) The ultimate capacity of the cable exceeded the minimum expected capacity.

(d) Destructive examination of the socketed wire demonstrated that the internal layers of wire experience no adverse conditions as a result of cable vibration. None of the rub marks showed any adverse condition nor were they comparable to the fretting marks observed in the outer wires that cracked.

(e) Failure of the externally broken wires was by fatigue crack growth starting at fretting marks on the wire surface. These failures are essentially identical to those first seen in 1981.

(f) It was not possible to remove the inner wire layers from the zinc poured into the socket without plastically deforming the wires.

(g) Some small regions of the internal layers were found to lack zinc coating as a result of the socketing. Apparently, the removal of galvanizing material from the wires prior to pouring resulted in some wires not being coated completely when socketed. Some corrosion product was observed in these regions.

(h) The existing cables can be safely used in the structure without concern for the fatigue resistance and ultimate capacity.

2. Samples Removed from Diaphragm and Weld Connection to Outer Web

(a) Fatigue crack growth was detected in all weld cracks examined. The rate of crack propagation was relatively high which is not unusual for a random variable load history.

(b) Some evidence of ductile crack extension was observed in several weld cracks taken from the bottom end of the connection. This suggested that large loads were introduced into the weld connection during the initial stages of crack extension. It seems probable the construction forces caused some of this condition as well as wind induced cyclic stresses.

(c) The lack of fusion between the fillet weld roots of the diaphragm-web weld connection promoted crack extension under repeated loads.

3. Strain Measurements and Assessment of Cracking

(a) The strain measurements from controlled traffic demonstrated that significant cyclic stresses are introduced into the diaphragm - web welded connection and the tie girder web gaps as a result of the end restraint at the floor beam - tie girder connections.

(b) Strain measurements of the gages installed on the diaphragm and in the web gap also demonstrated that significant cyclic stresses developed as a result of aeroelastic response of the structure at wind velocities of 30, 35, and 40 mph. These cyclic stresses were at times larger than the response observed from the controlled load test trucks.

(c) From the observed initial lack of fusion condition that existed at the weld crack samples, the crack growth threshold would be exceeded by a stress range of 2 or 3 ksi.

(d) The striation spacing observed in the weld crack of sample 3'S indicated that the crack growth rate was relatively high. The estimated stress intensity range was between 25.5 and 33.9 ksi $\sqrt{in}$.

(e) All cracks in the diaphgram - web weld connections lie in a plane that is parallel to the primary stresses in the tie girder. These cracks do not affect the strength and integrity of the structure.

(f) The structure can be opened to traffic prior to carrying out corrective action. Retrofitting should be carried out in the near future, so that crack growth is minimized.

(g) The tie girder floor beam diaphgram - web welded connections and weld cracks should be inspected at a four to six week interval pending completion of the retrofit.

(h) The web gap strain measurements demonstrated that high out-of plane web bending stresses are introduced into the web. These cyclic stresses are particularly high when projected to the weld at the root of the backing bar. Hence, cracking can develop at the root in the web flange weld as a result of these stress cycles. All four box corners would be susceptible. However, those without interior fillet welds will be more adversely affected than those with the fillet welds attaching the backup bar to the web and flange.

(i) These cracks will be parallel to the primary stresses in the tie girder and do not affect its resistance. Examination of the root area after several backup bars were removed confirmed that some crack extension had developed at the root of the backing bar.

4. Studies of Cracked Hanger Support Angle

(a) The cracking observed in the A517 steel angle was found to be a mixture of hydrogen induced cold cracking and lamellar tearing.

(b) Part of the crack developed during fabrication before the section was painted.

(c) Small regions of fatigue crack extension were detected near the preexisting crack tips.

TABLE 1 SUMMARY OF FATIGUE TESTS ON 2-1/4 IN. STRAND

Specimen	Location	Min. Load kips	Max. Load kips	Nominal Stress Range	Cycles
B*	7NW-Top	132	174	14	4,789,400
C	5NW-Bottom	132	174	14	4,836,900
D*	8SE-Bottom	132	164	10	4,192,800
E	8SE-Top	132	164	10	3,826,000
F	8SE-Center	132	152	7	5,140,600

*Broken Wires Detected Prior to Testing

TABLE 2 TENSILE TESTS ON WIRES FROM CABLE 7SW

Specimen	Load (kips) @ 0.7% Elong.	Yield Stress (ksi) @ 0.7% Elongation	Ultimate Load kips	Tensile Strength (ksi)	% Elongation
1	5.1	185	6.4	233	6.7
2	5.2	189	6.4	233	6.33
3	5.1	185	6.5	236	8.5
4	4.7	171	6.3	229	7.33

TABLE 3 ULTIMATE LOAD TEST RESULTS

OF FATIGUE TESTED CABLES

Specimen	No. of Orig. Broken Wires	Ultimate Load, kips	No. Wires Broken
A	0	573	26
D	3	520.5	12
E	0	578.5	20

TABLE 4 SUMMARY OF ESTIMATED STRESS RANGES

AT WELD TERMINATIONS - RUN 18

Panel Point	Outside Web				Inside Web
	Top Gap		Bottom Gap		Bottom Gap
	Diaphragm	Backing Bar	Diaphragm	Backing Bar	Backing Bar
4'	5 ksi	4.5 ksi	4.5 ksi	8 ksi	10-15 ksi
8	6.2 ksi	4 ksi	3 ksi	5.5 ksi	3 ksi

TABLE 5 SUMMARY OF MAXIMUM STRESS RANGE FOR TEST RUNS

Test Run	Direction	Vel. mph	Stress Range ksi B11 Inside Web 4'	B8 Outside Bottom 4'	B4 Outside Top 4'	A4 Top Outside 8
1	E	30	4.1	2.9	1.3	1.6
2	W	30	3.5	2.5	1.6	2.4
3	E	30	4.4	3.3	1.6	2.1
4	W	30	4.1	2.7	1.7	2.2
5	E	30	5.9	4.9	2.5	3.2
6	W	30	--	--	--	4.
7	E	50	4.3	2.7	1.8	2.
8	W	42	--	--	--	--
9	E	40	4.5	3.4	1.6	2.2
10	W	35	4.	2.8	1.8	2.6
11	E	40	7.1	5.	2.6	3.2
12	W	40	6.4	4.5	2.6	4.2
13	E	45	5.5	3.9	1.7	1.9
14	W	55	4.5	2.9	1.9	2.2
15	E	48	4.8	3.4	1.9	2.1
16	W	60	4.4	3.2	1.9	2.7
17	E	45	7.	4.8	2.5	3.2
18	W	45	6.2	4.1	2.5	4.1

TABLE 6 SUMMARY OF STRESS RANGE IN DIAPHRAGM

ADJACENT TO FILLET WELDS - RUN 18

Panel Point	Top of Diaphragm	Bottom of Diaphragm
4'	5.3 ksi	0.6 to 2.8 ksi
8	5.5 ksi	1.2 ksi

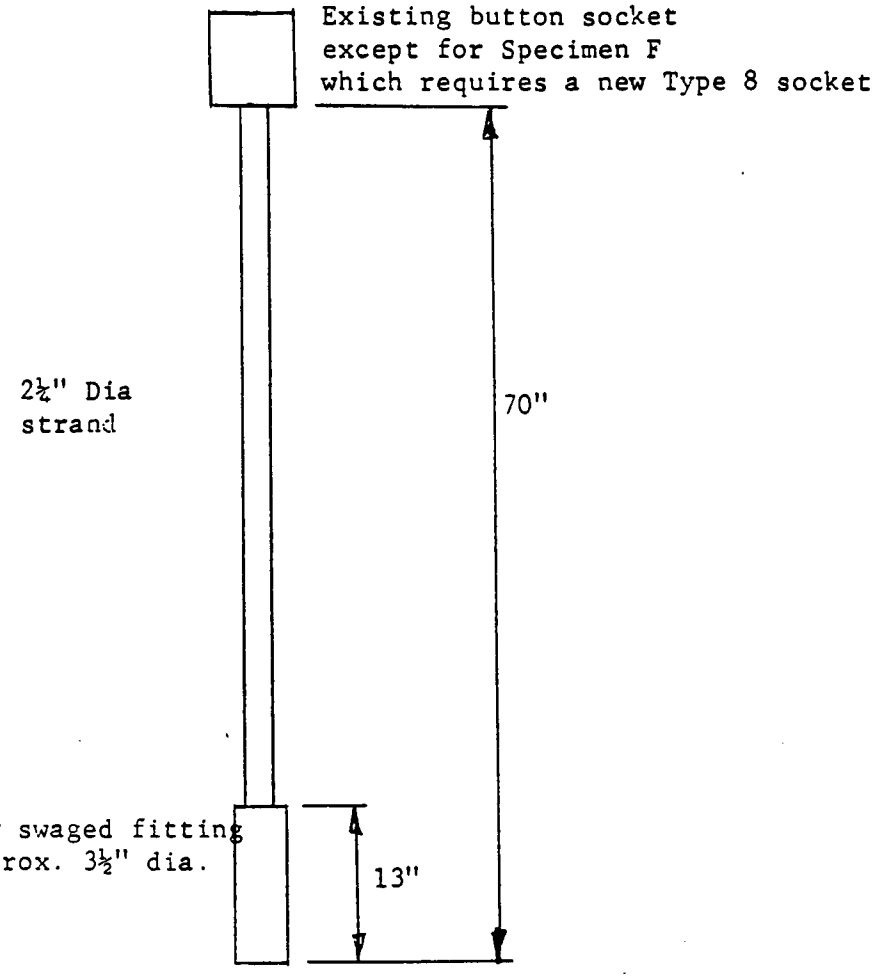

Specimen	To be cut from cable	Location
A	7SW-Top	Tie end with 4 broken wires
B	7NW-Top	End with broken wires
C	5'NW-Bottom	End without broken wires
D *	8SE-Bottom	Tie end with broken wires
E	8SE-Top	End without broken wires
F **	8SE	Center of cable

* Outer layer of wires to be removed for testing

** This specimen requires a new Type 8 socket

Fig. 1 Schematic and Designation of Test Specimens

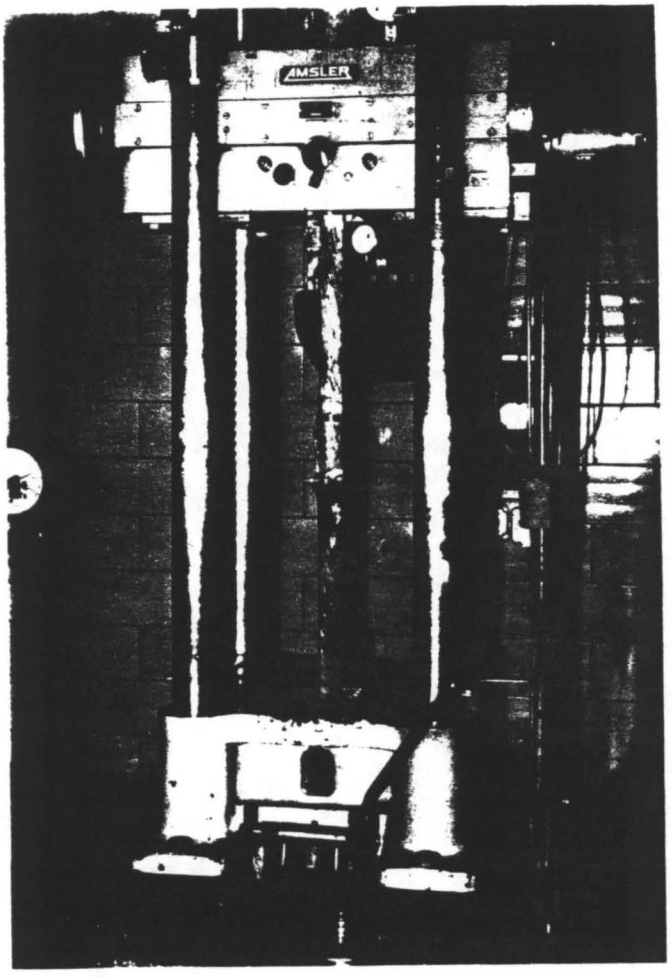

8/83/16-20

Fig. 2 Cable Under Test in the Alternating Stress Machine

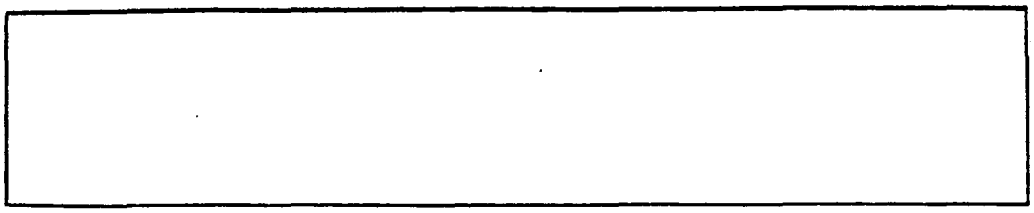

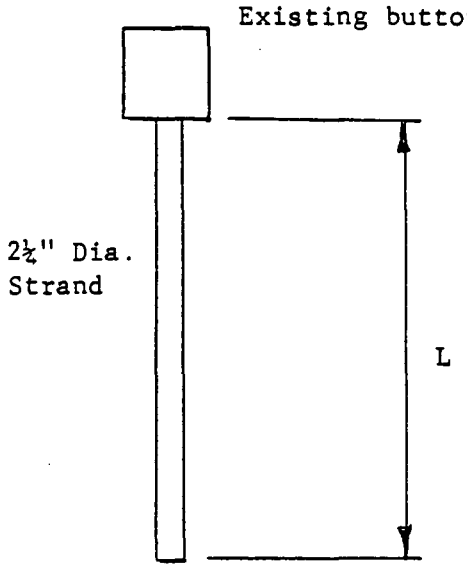

Specimen	To be cut from cable	Length L	Location
G	7SW -Bottom	36"	End without broken wires
H	5'NW -Top	36"	End with broken wires
I	5'NE -Top	36"	End with broken wires
J	5'NE -Bottom	70"	End without broken wires

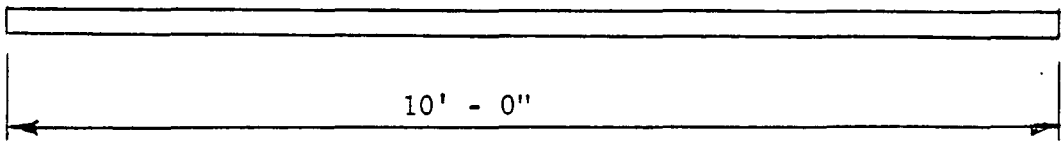

Specimen K To be cut from cable 7SW from a region near the center where significant rubbing of wires from vibration has occurred

Fig. 3 Schematic of Cable Segments for Destructive Examination

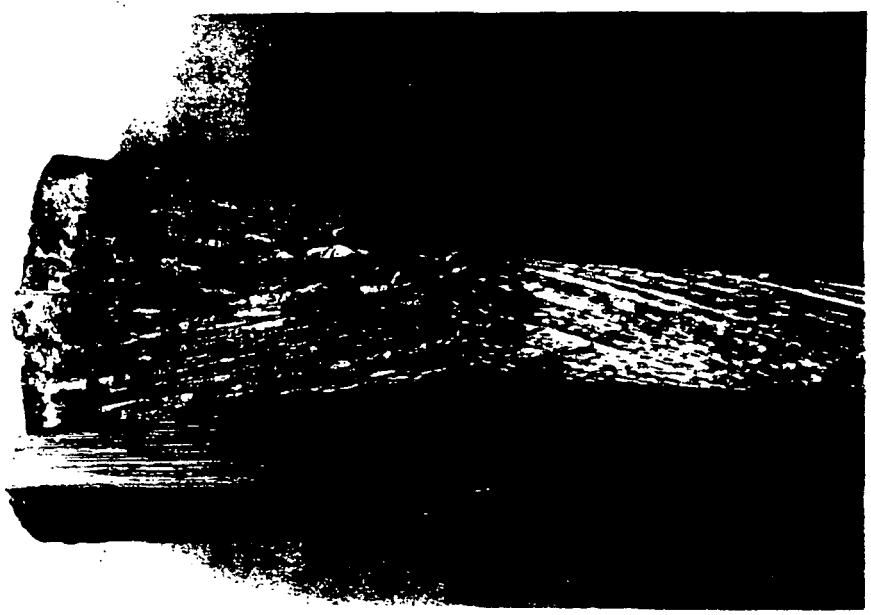

7/83/3-12

(a) Exposed Socketed End

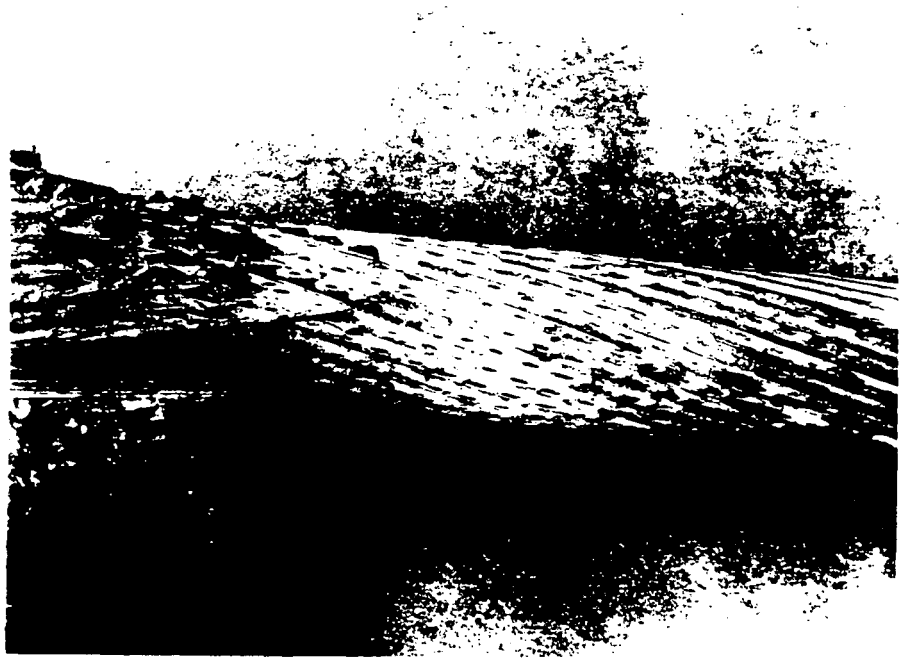

7/83/4-14

(b) Exposed End at End of Socket

Fig. 4 Cable and Saw Cut Socket

9/83/40-19

Fig. 5 Wire I-1 Side View of Fracture

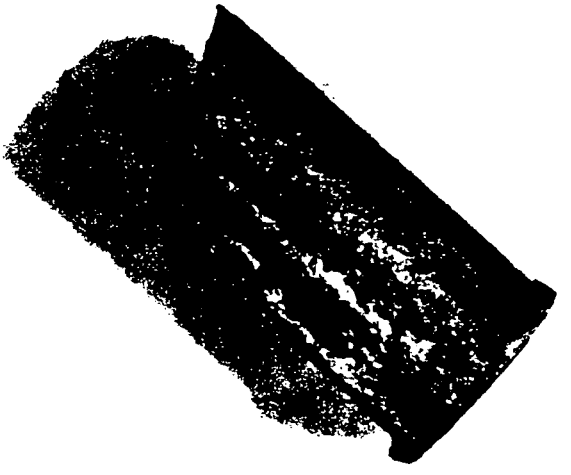

7/83/14-13

Fig. 6 Wire I-1 Side View of Fracture

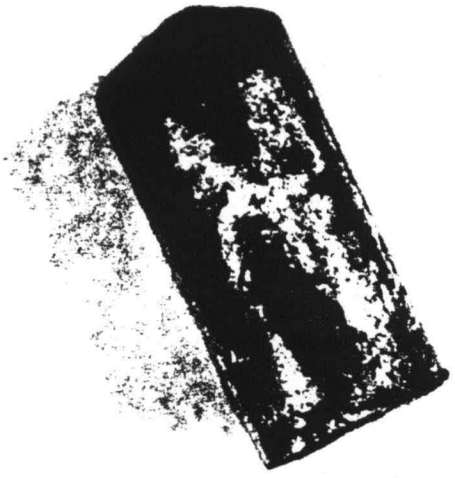

7/82)15-17

3

Fig. 7 Wire I-1 Side View of Fracture Showing Gouge Marks

7/82)12-10

4 21

Fig. 8 Wire I-1 Fracture Surface (not cleaned)

Fig. 9 Wire I-1 SEM Micrograph of
Fracture Surface (not cleaned), 20X

Fig. 10 Wire I-1 SEM Micrograph of
Fracture Surface (cleaned), 20X

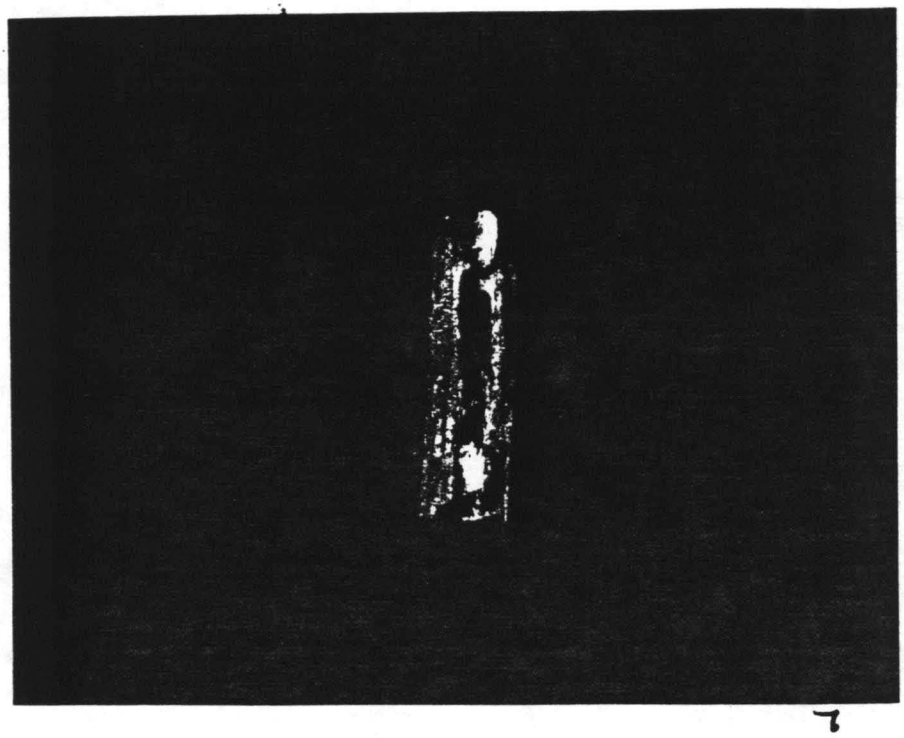

9/83/40-20

Fig. 11 Wire H-1 Side View Showing Fracture and Associated Gouge Marks

Fig. 12 Wire H-1 SEM Micrograph of Fracture Surface (cleaned), 20X

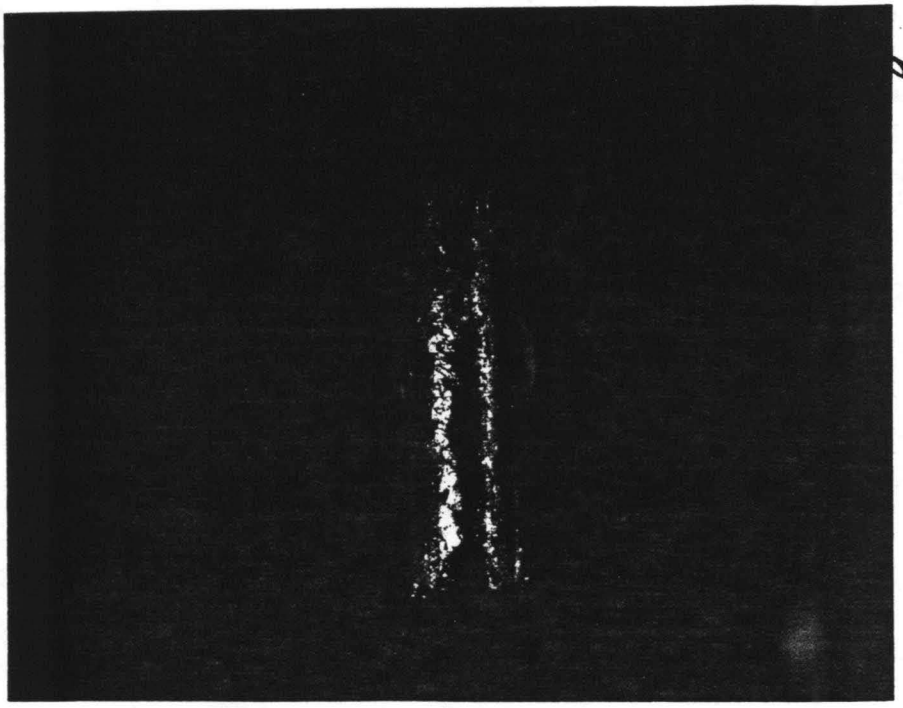

9/83/42-6A

Fig. 13 Wire D-1 Side View of Fracture (on right), Showing Gouge Marks

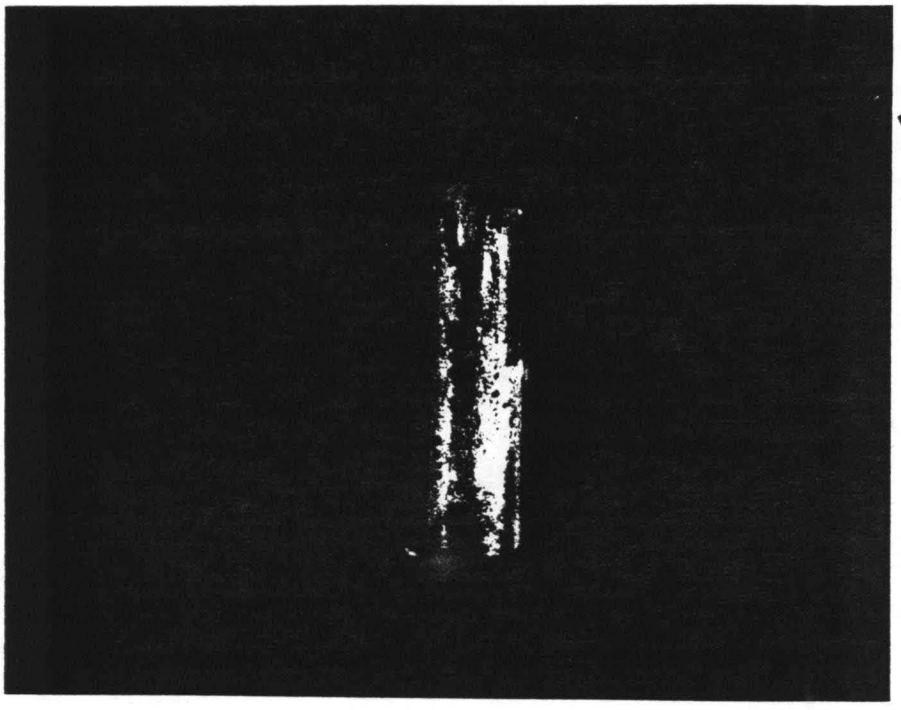

9/83/41-3A

Fig. 14 Wire D-2 Side View of Fracture (on right), Showing Gouge Marks

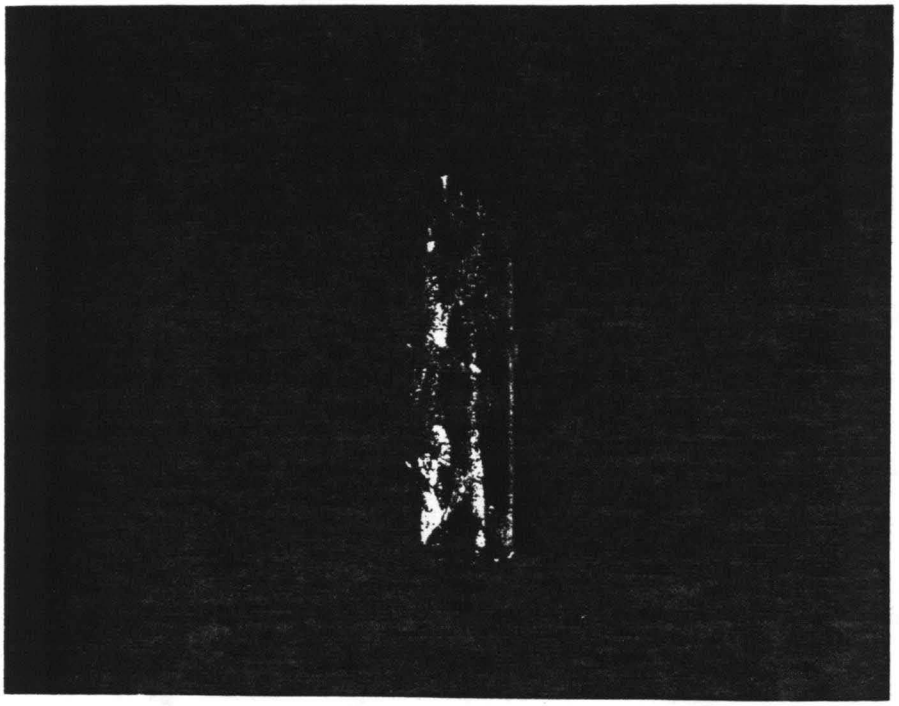

9/83/41-1

Fig. 15 Wire D-3 Side View of Fracture (on right), Showing Gouge Marks

Fig. 16 Wire D-1 SEM Micrograph of Fracture Surface Showing Beach Marks (cleaned), 10X

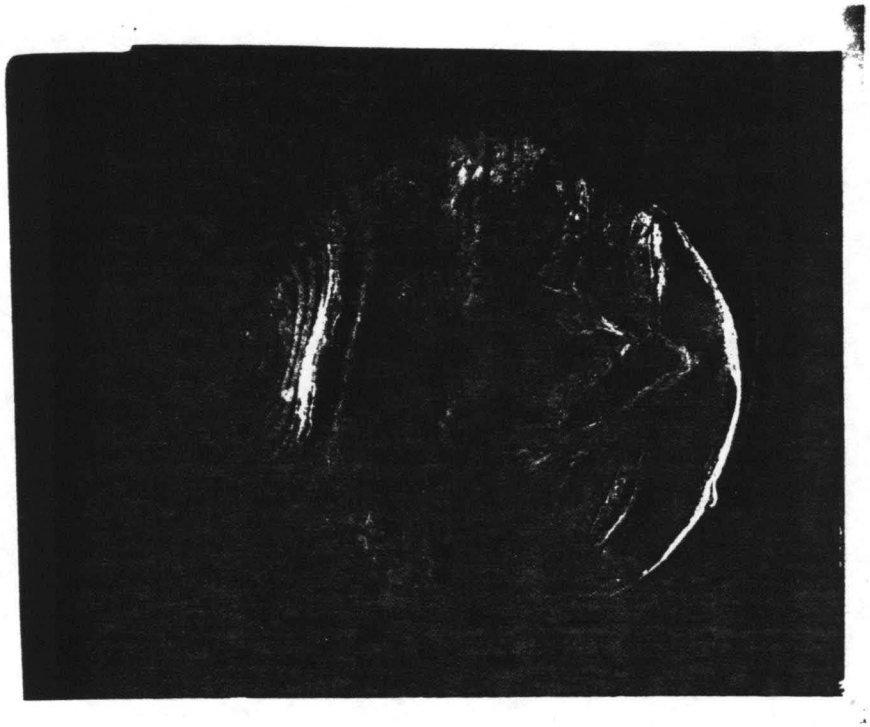

Fig. 17 Wire D-2 SEM Micrograph of Fracture Surface Showing Beach Marks (cleaned), 10X

Fig. 18 Wire D-3 SEM Micrograph of Fracture Surface Showing Beach Marks (cleaned), 10X

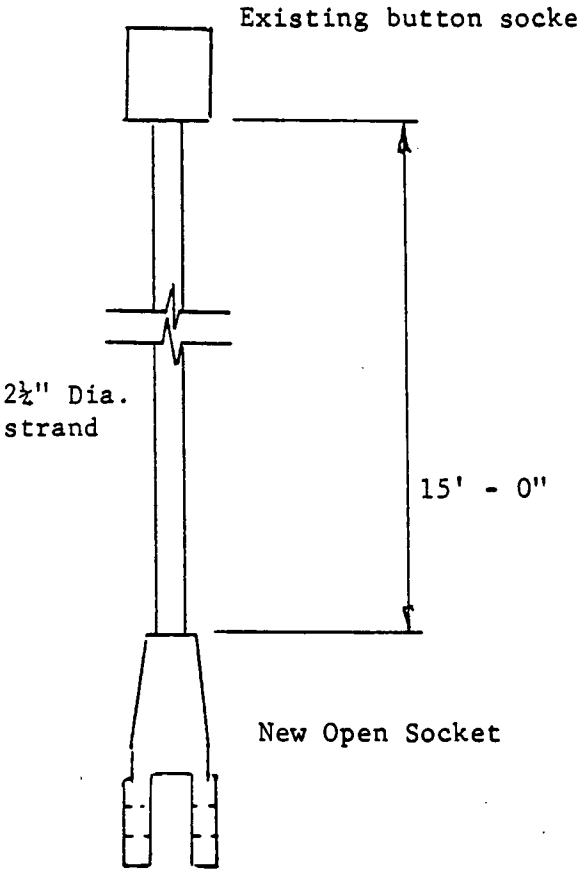

Specimen L To be cut from cable 7NW from the end without broken wires

SUMMARY OF NEW SOCKETS REQUIRED: 6 Swaged Sockets
1 Type 8
1 Open Socket

Fig. 19 Schematic of Tensile Test Specimen

FRITZ ENGINEERING LABORATORY

Lehigh University

File 200.83.479.1

Sheet ..... of .....

Subject MAJESKI + MASTERS

TEST OF 2 1/4" STRAND

Date 7/14/83

Party RD

JW

Approved .....

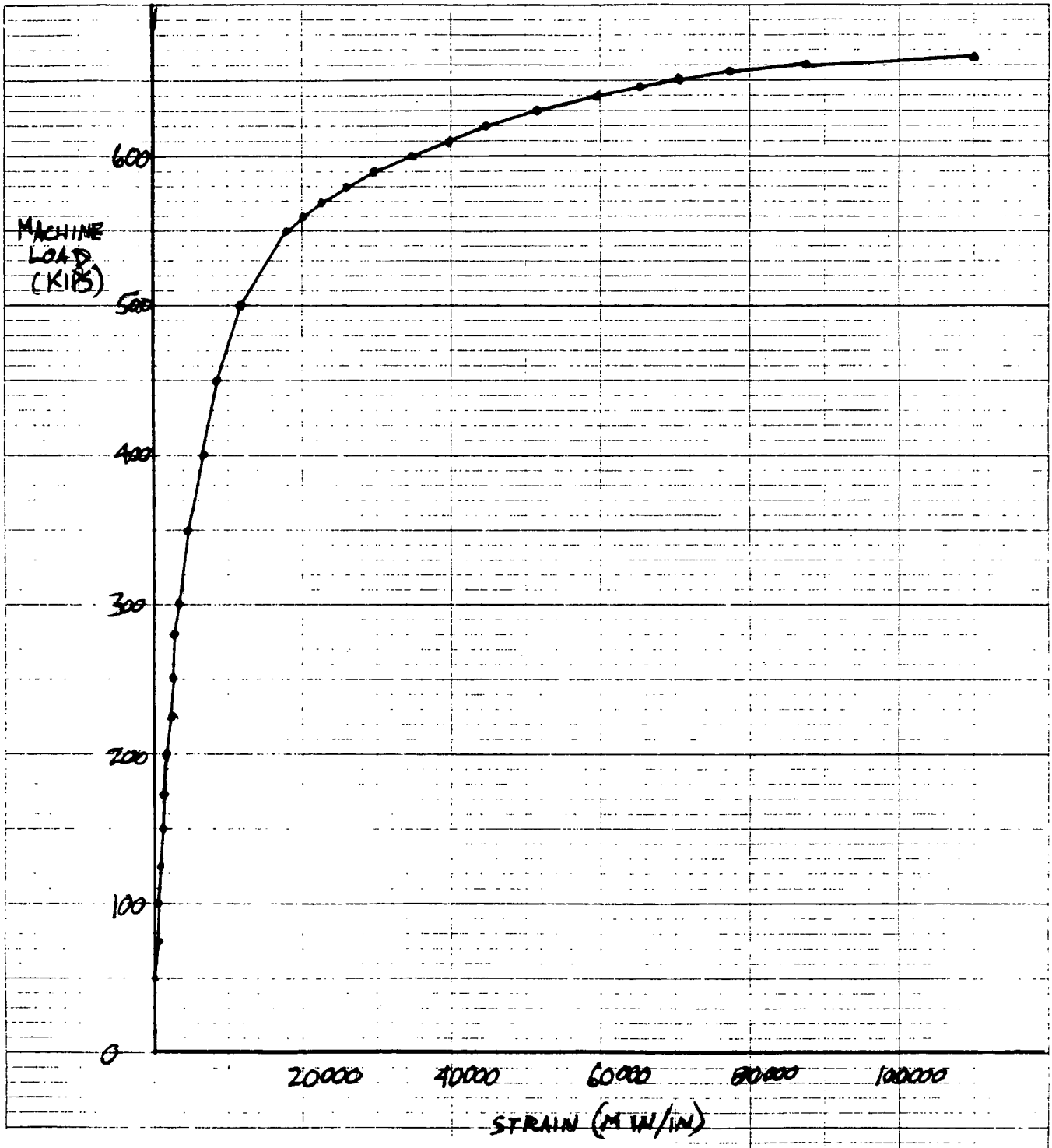

Fig. 20 Load-Strain Curve for Tensile Specimen

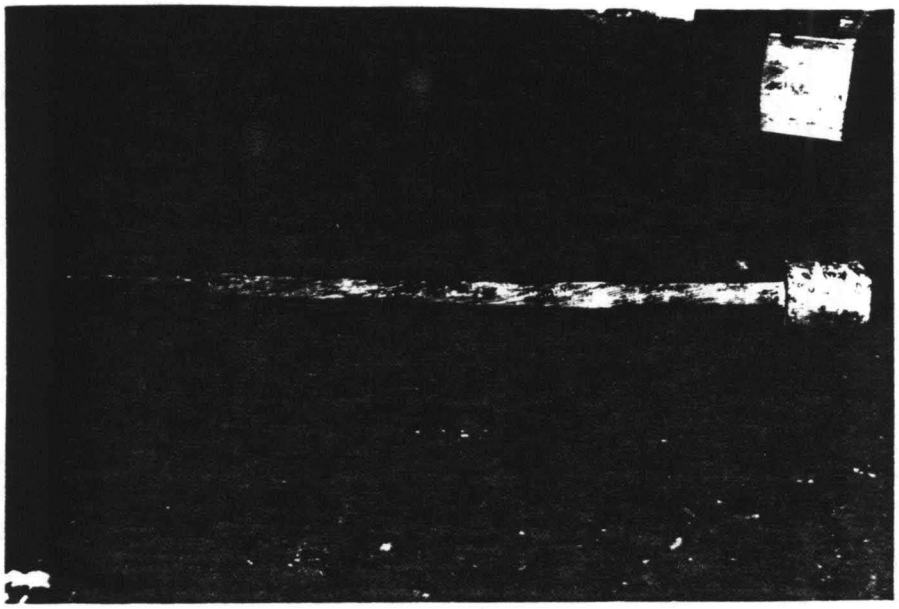

10/83/1-11

Fig. 21 Fatigue Test Specimen with Original Button Socket and New Swagged Fitting

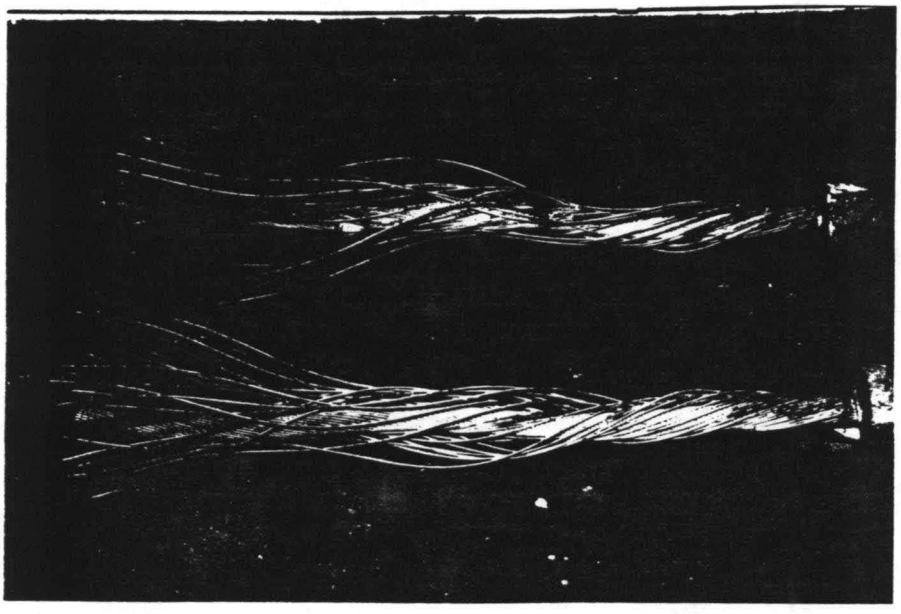

2/84/1-8

Fig. 22 Specimens D and E After Failure

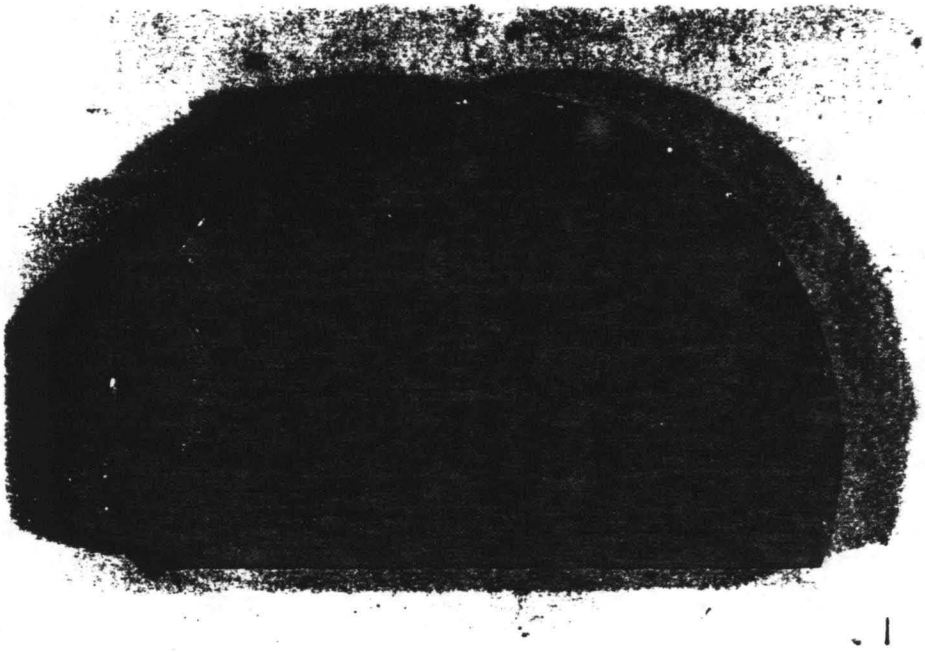

8/83/45-19

Fig. 23 Sample 3'N

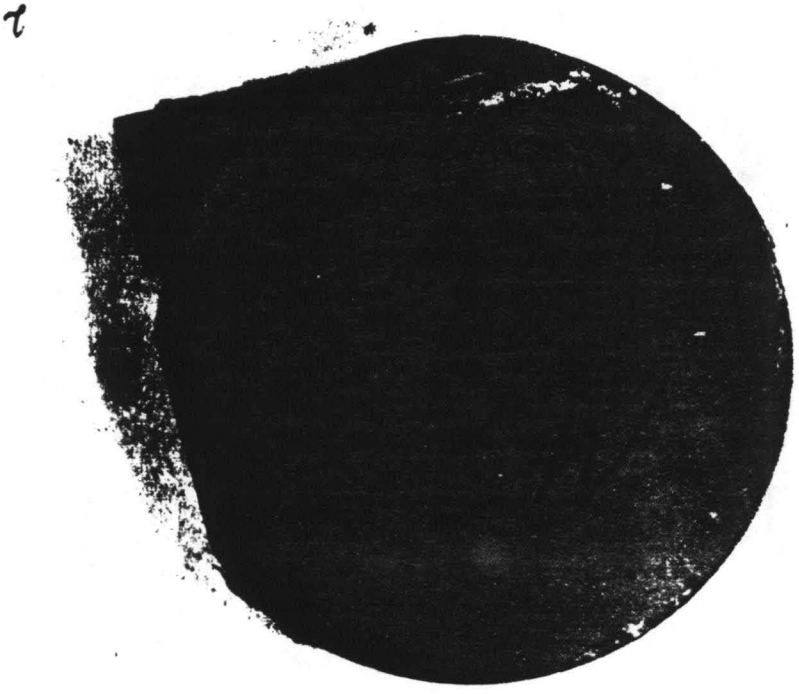

9/83/5-20

Fig. 24 Sample 6N

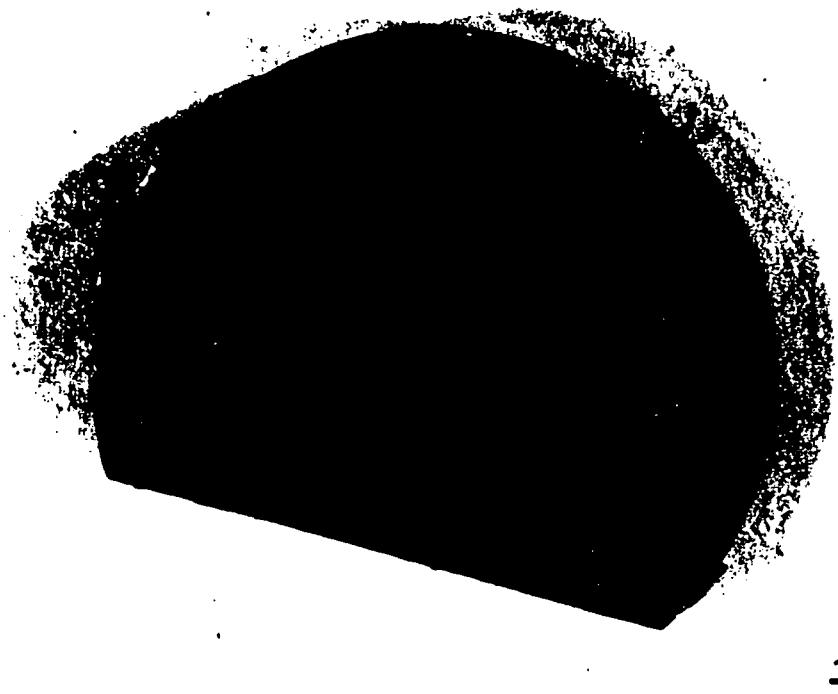

9/83/3-13

Fig. 25 Sample 6'N

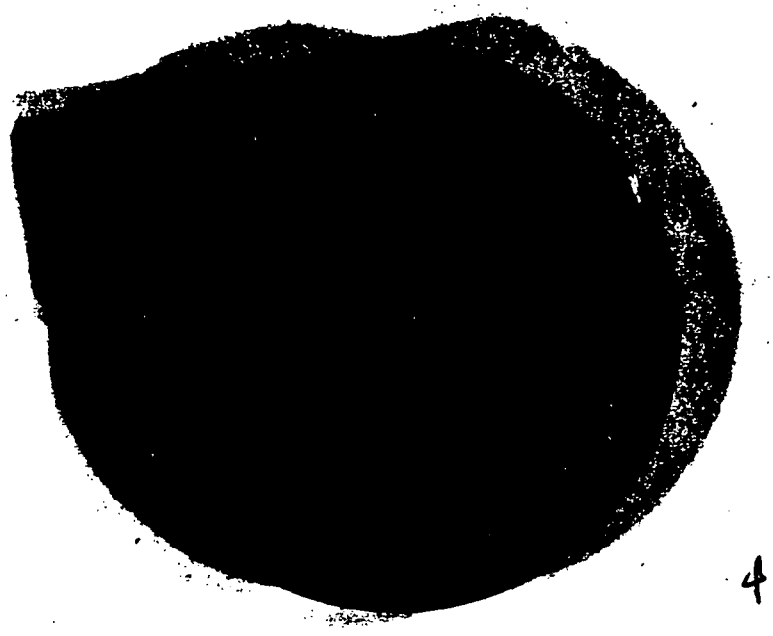

8/83/43-10

Fig. 26 Sample 3'S (Note: Segment was incorrectly identified as 3'N)

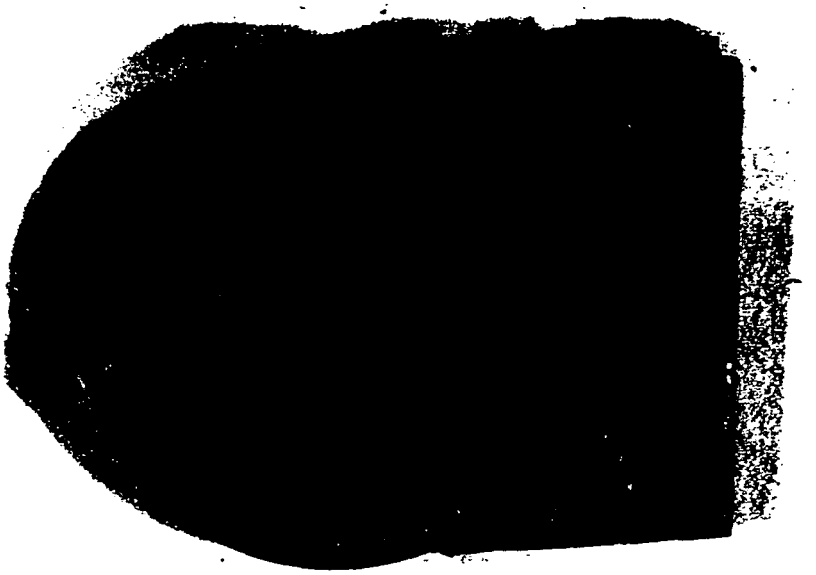

8/83/44-15

5

Fig. 27 Sample 4'S

9/33/2-15

6

Fig. 28 Sample 8S

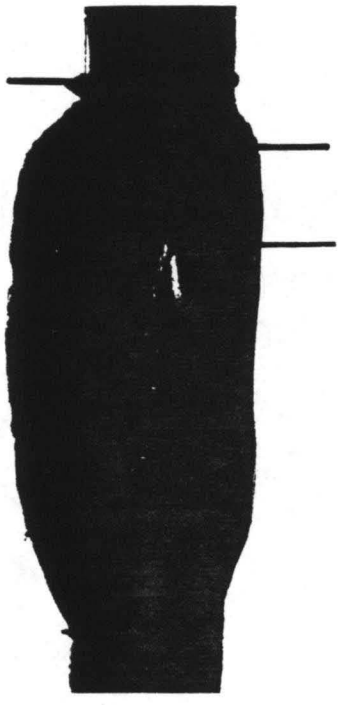

9/83/49-10A

Fig. 29 Etched Weld Root Area on Sample 3'S

9/83/49-9A

Fig. 30 Etched Weld Root Area on Sample 4'S

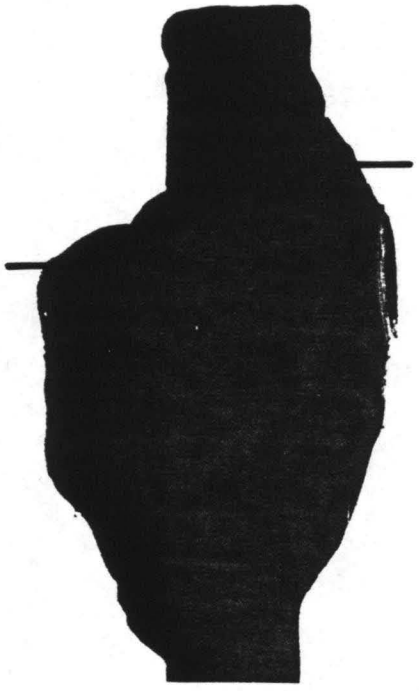

9/83/49-11A

Fig. 31 Etched Weld Root Area, on Sample 6'N

9/83/10

Fig. 32 SEM Micrograph of Sample 4'S, 1500X

9/83/11

Fig. 33 SEM Micrograph of Sample 4'S, 600X

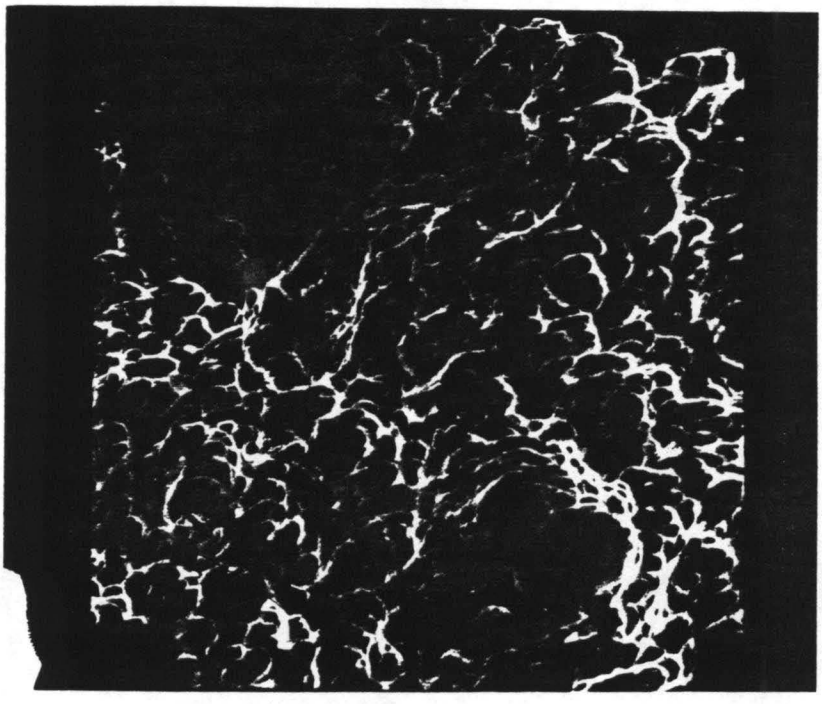

9/83/14

Fig. 34 SEM Micrograph of Sample 4'S, 1400X

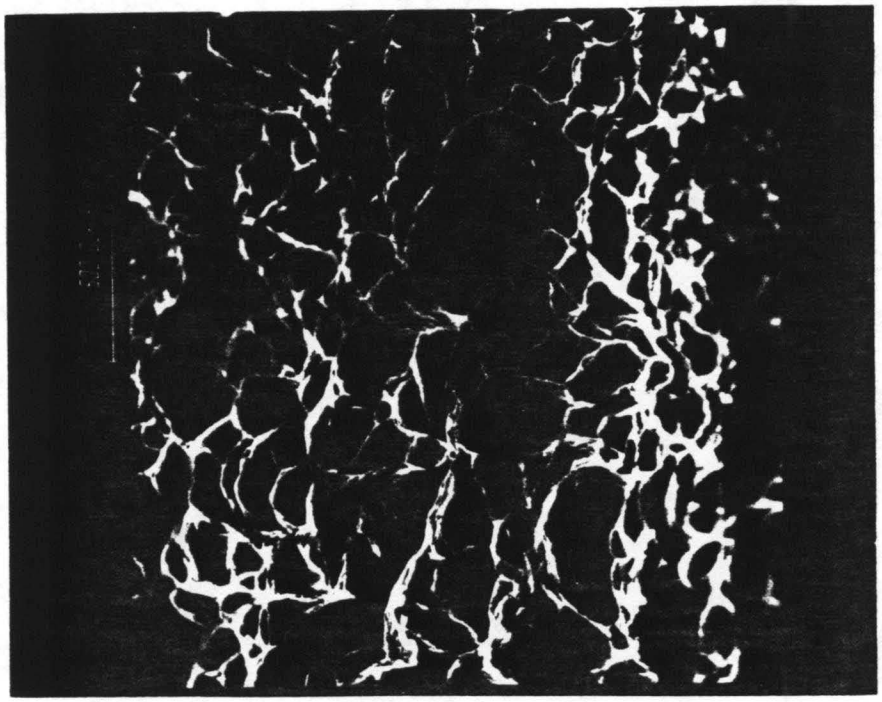

9/83/52

Fig. 35 SEM Micgrograph of Sample 6N, 2500X

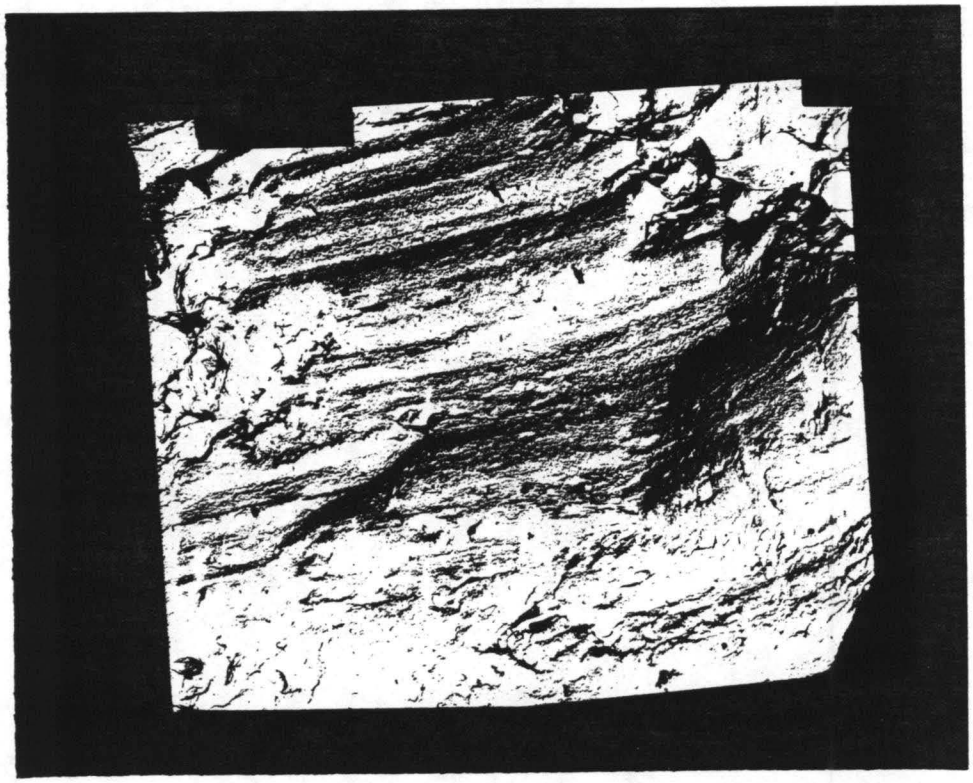

9/83/55

Fig. 36 TEM Micrograph of Sample 3'S, 5000X

9/83/02

Fig. 37 TEM Micrograph of Sample 3'S, 5000X

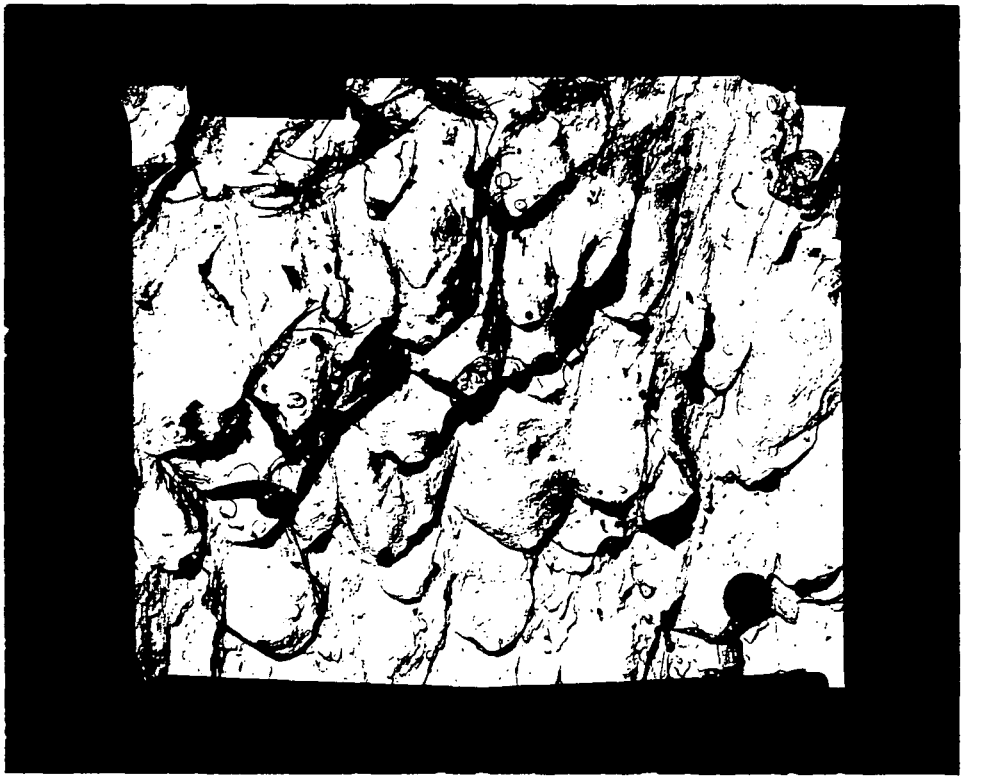

9/83/06

Fig. 38 TEM Micrograph of Sample 3'S, 6300X

9/83/18

Fig. 39 TEM Micrograph of Sample 3'S, 4000X

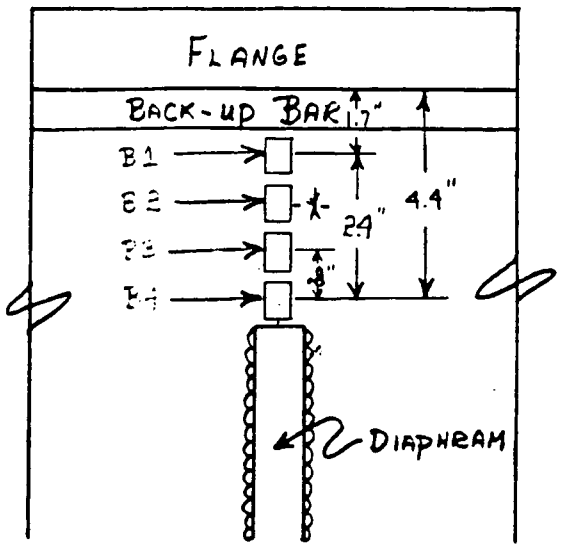

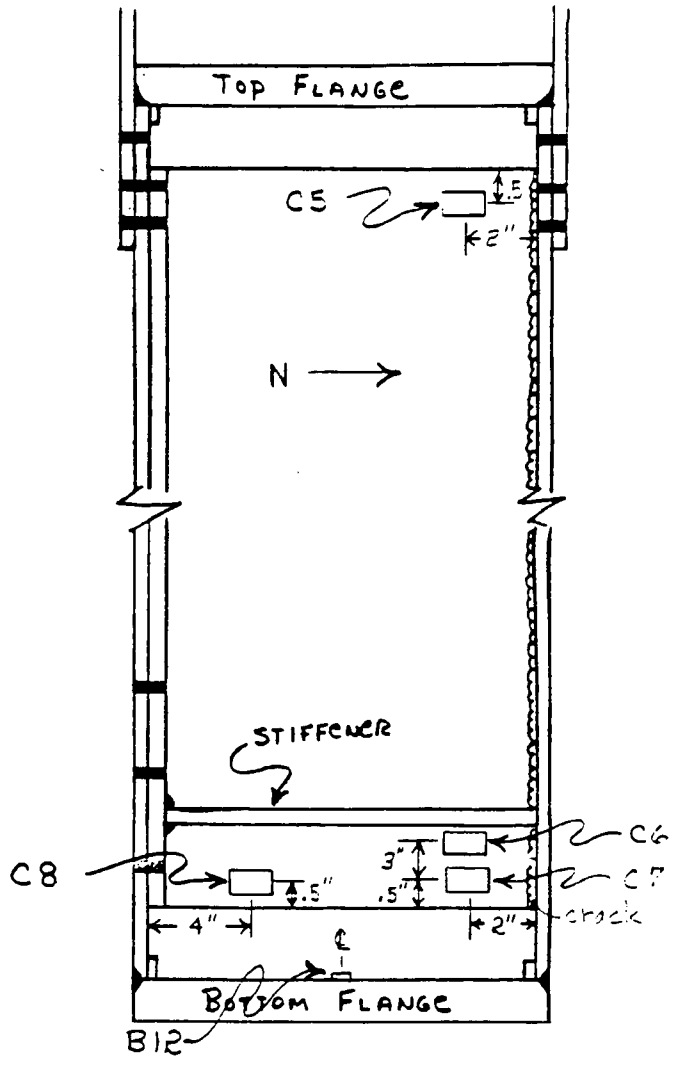

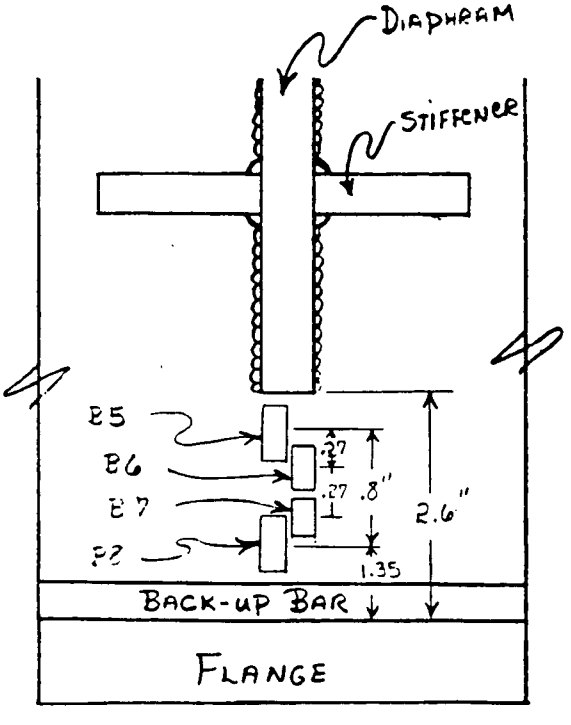

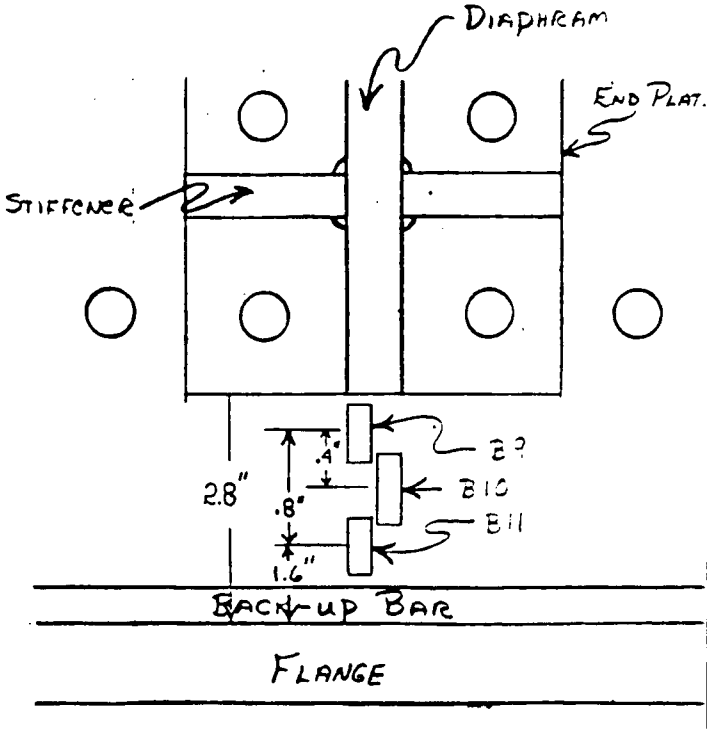

Fig. 40 Schematic Showing Strain Gage Locations at Panel Point 4'

(Rev. 3-74)
MADE BY K. NELSON DATE
CHECKED BY DATE
CALCULATIONS FOR PANEL POINT - E
PROJECT I-470
SHEET NO

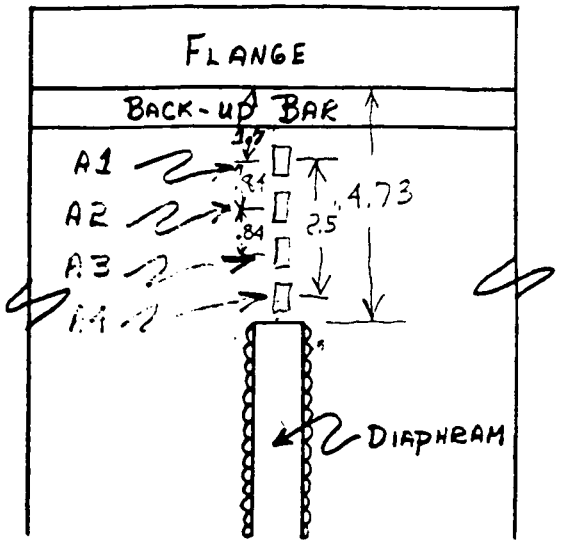

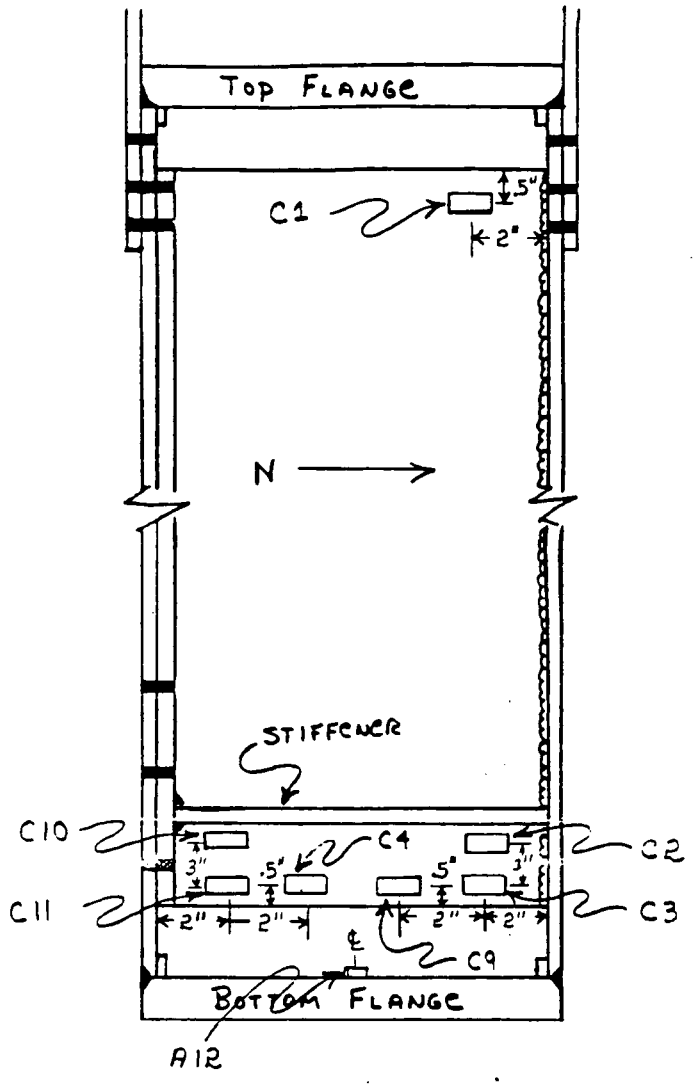

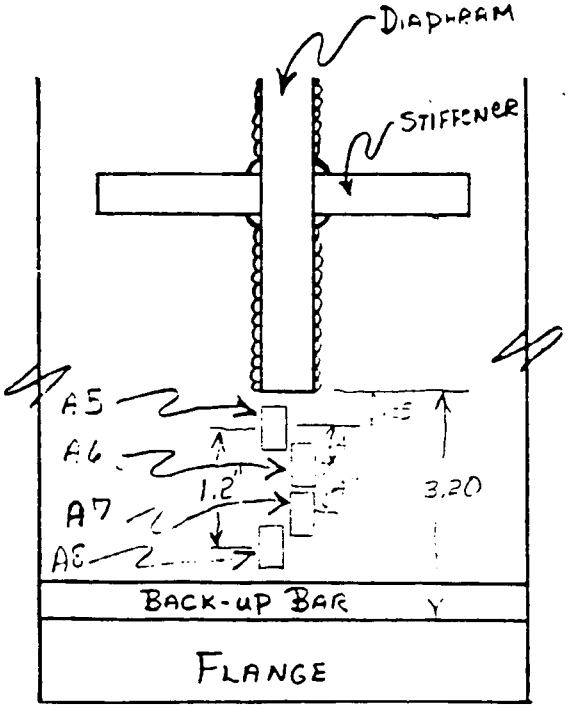

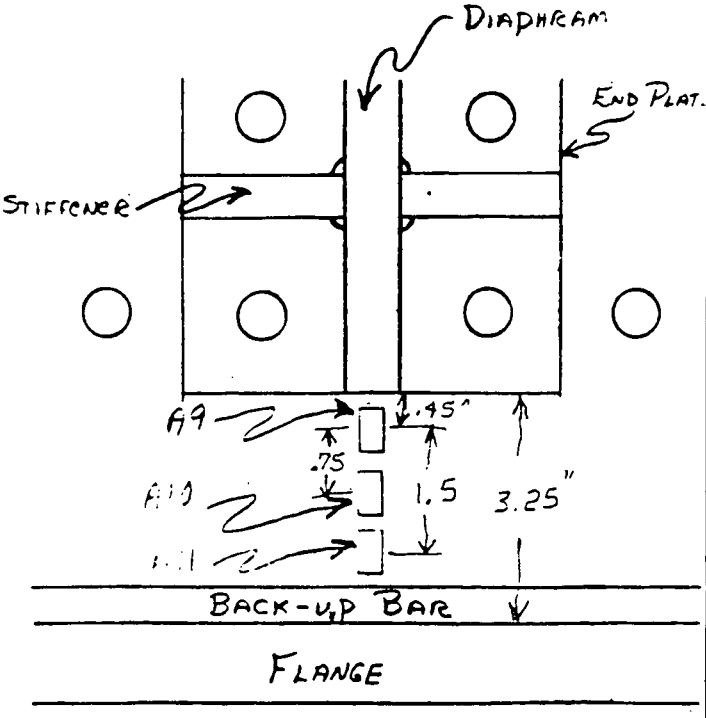

Fig. 41 Schematic Showing Strain Gage Locations at Panel Point 4'

PANEL POINT 8

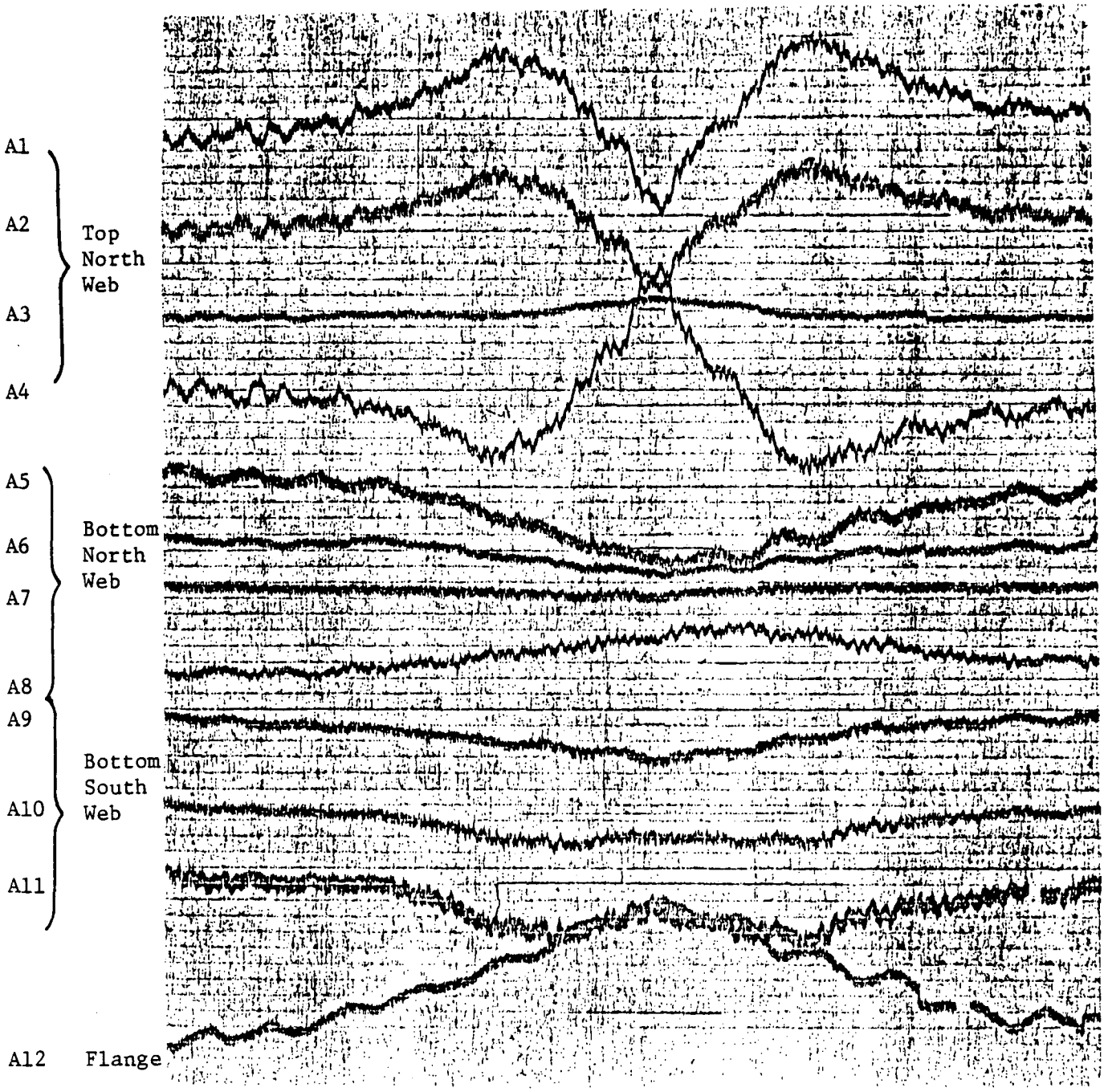

Fig. 42 Strain-Time Response Run 18 (WB) Panel Point 8

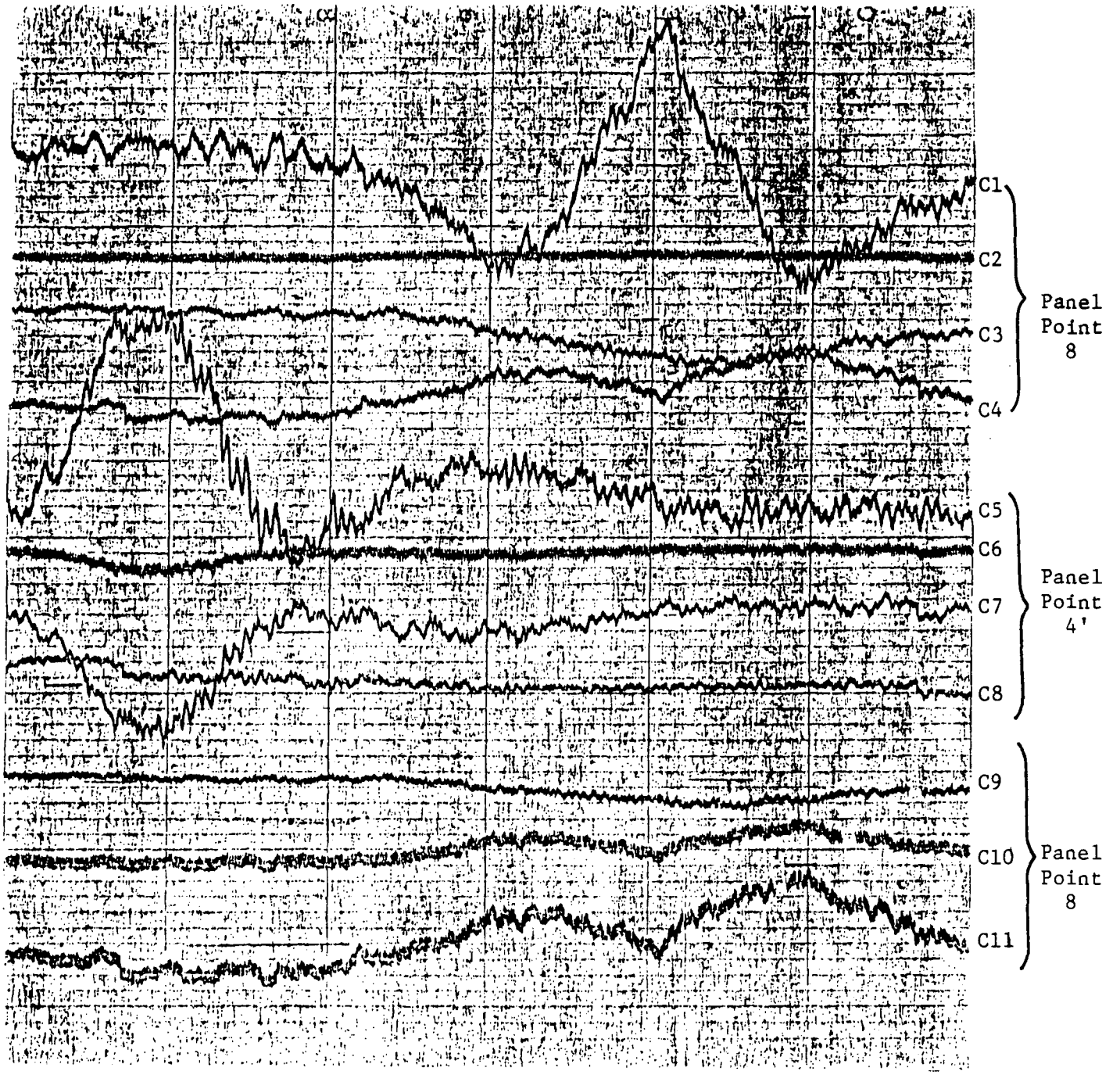

Fig. 43 Strain-Time Response Rune 18 WB Diaphragm at Panels 4' and 8

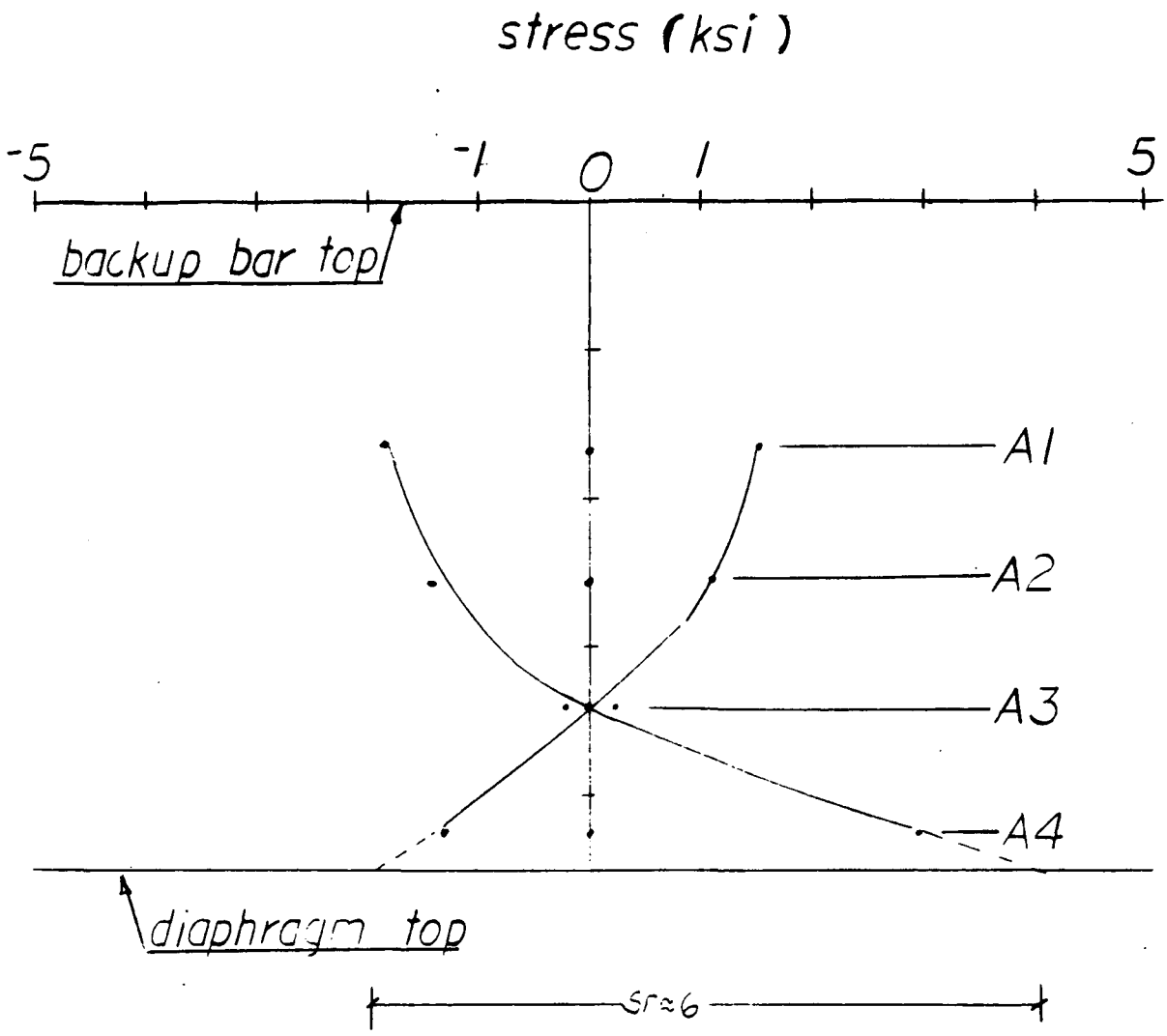

Fig. 44 Web Gap Stress Gradient in Region Adjacent to Top Flange - Outside Web Panel Point 8

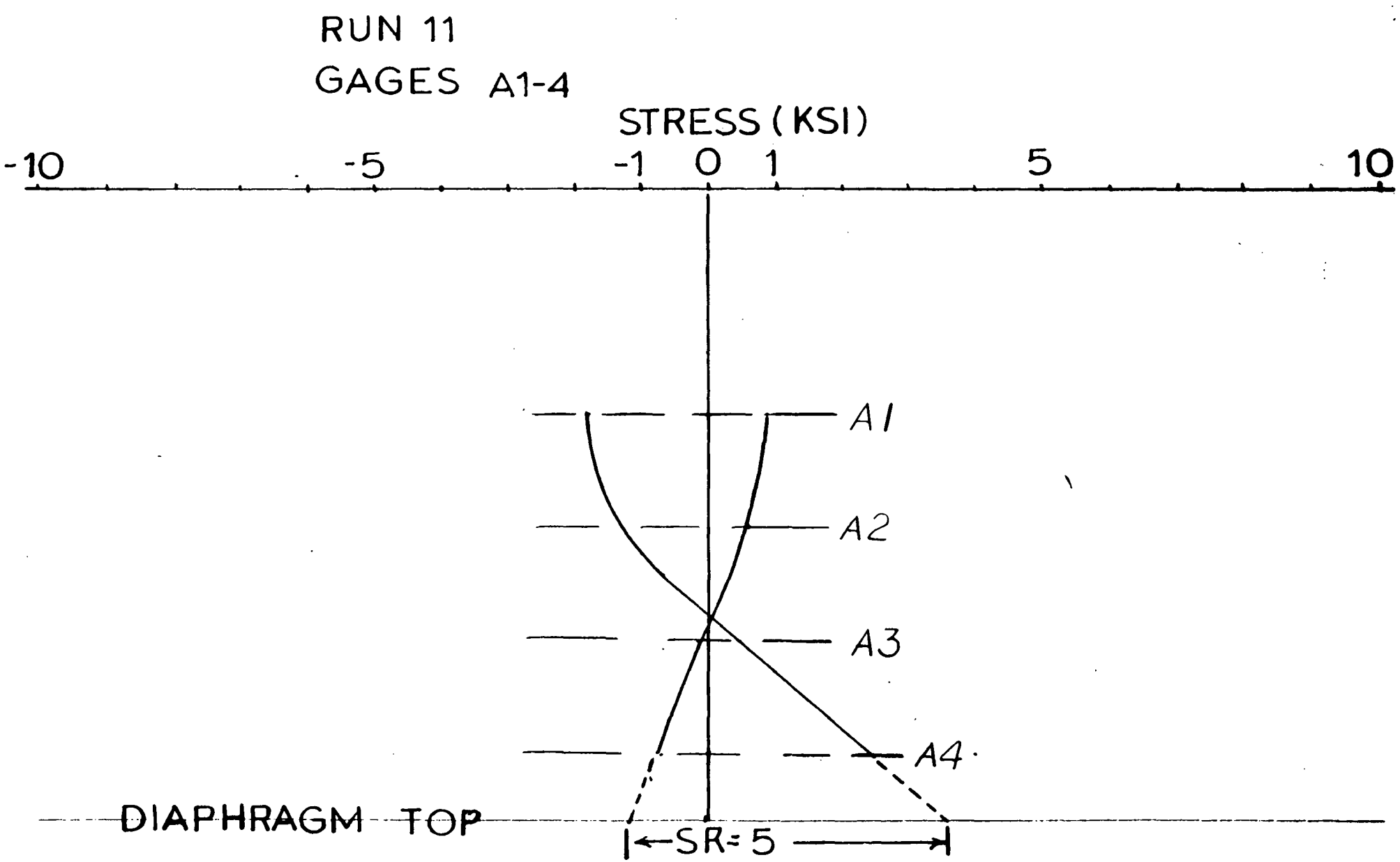

Fig. 45 Web Gap Stress Gradient in Region Adjacent to Top Flange - Outside Web of PP8, Run 11

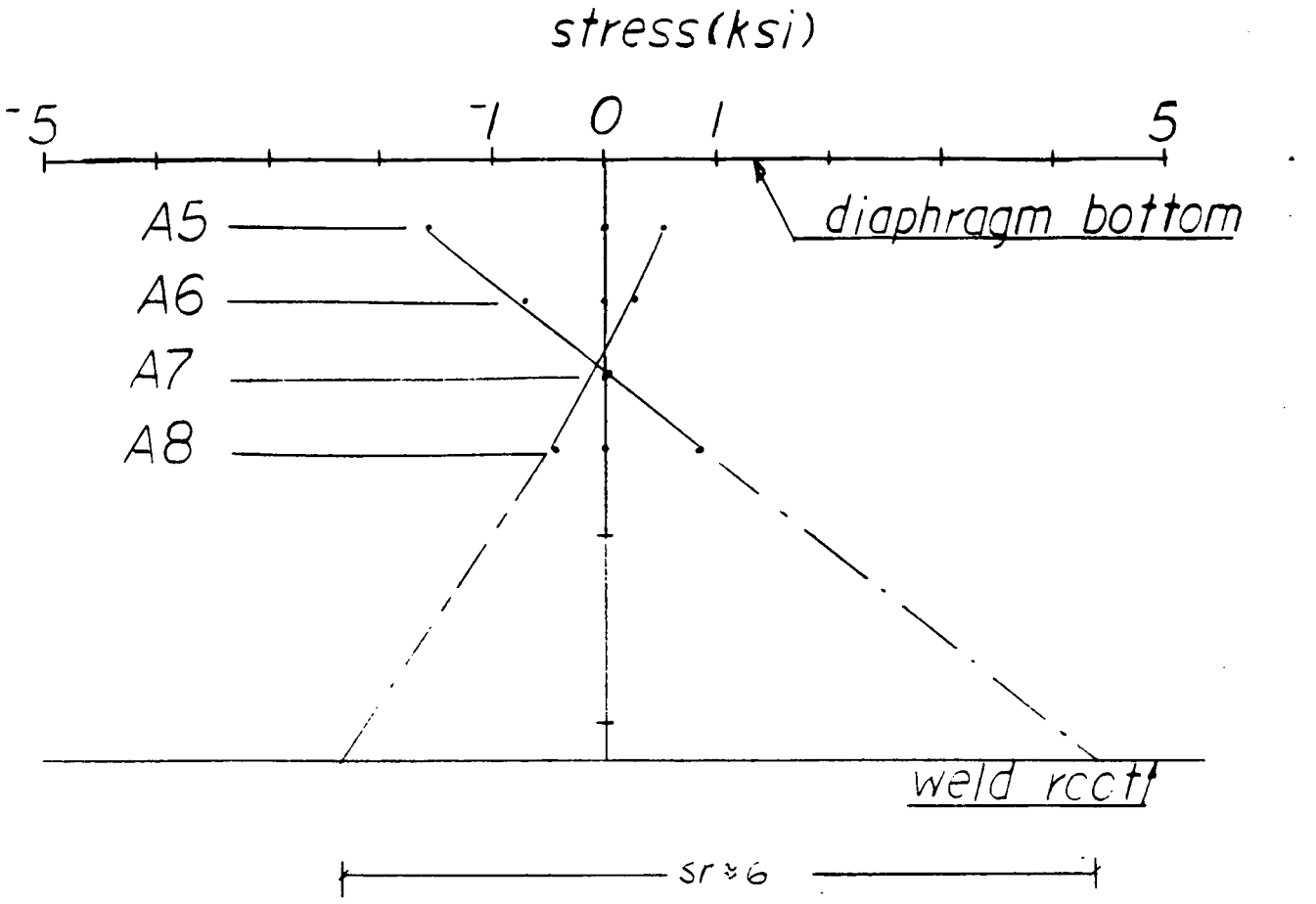

Fig. 46 Web Gap Stress Gradient in Region Adjacent to Bottom Flange - Outside Web Panel Point 8

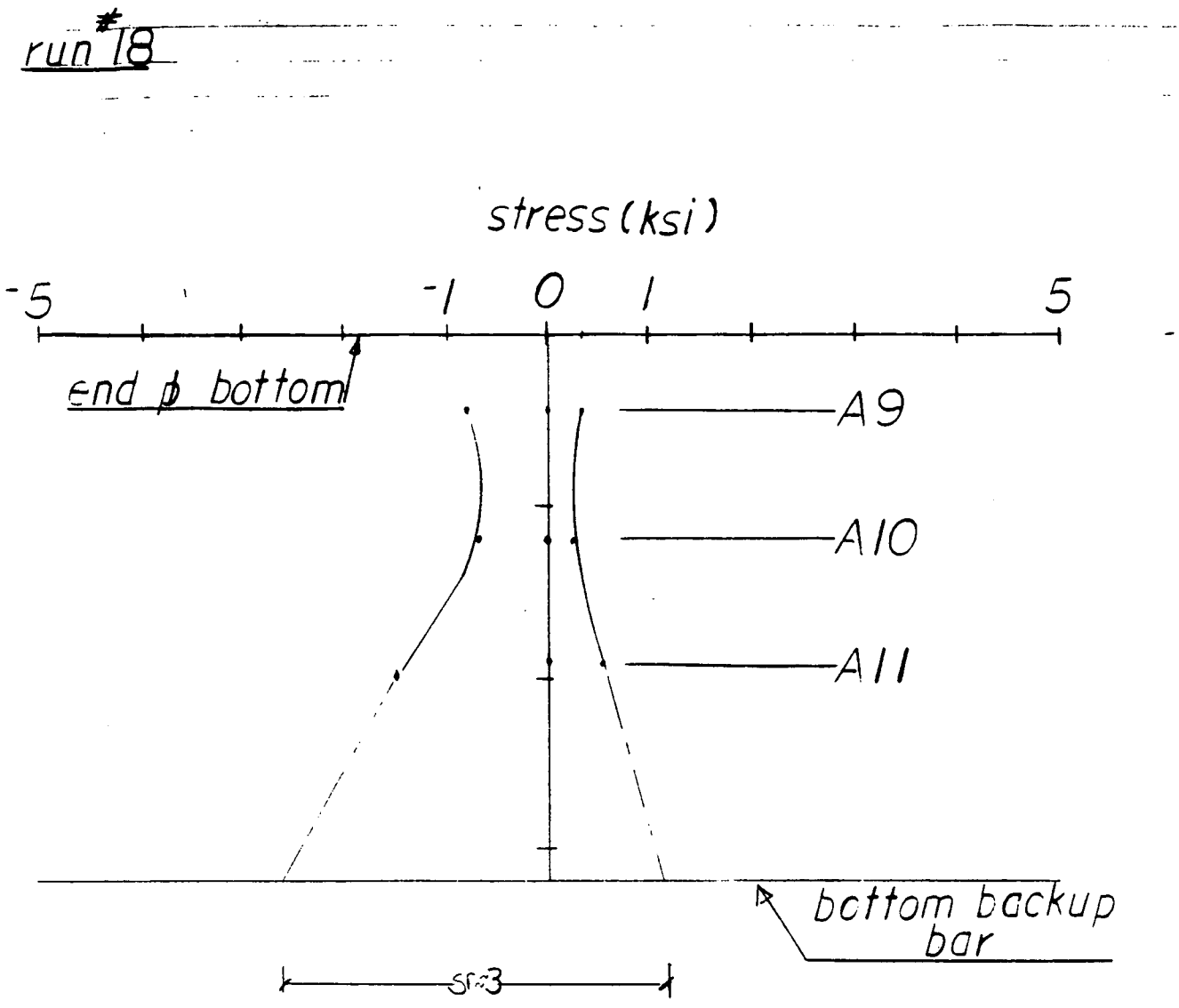

Fig. 47 Web Gap Stress Gradient in Region Adjacent to Bottom Flange - Inside Web Panel Point 8

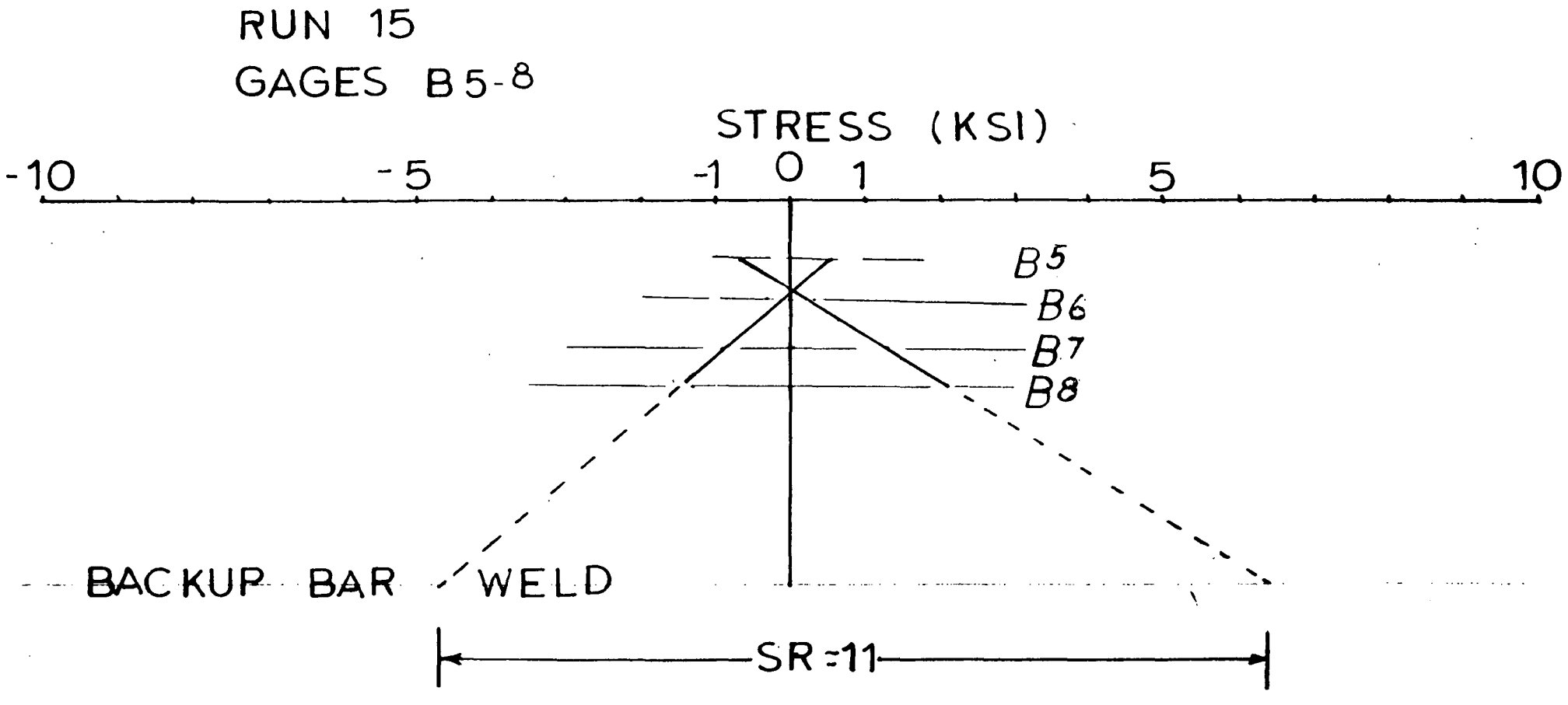

Fig. 48 Web Gap Stress Gradient in Region Adjacent to Bottom Flange - Outside Web of PP4', Run 15

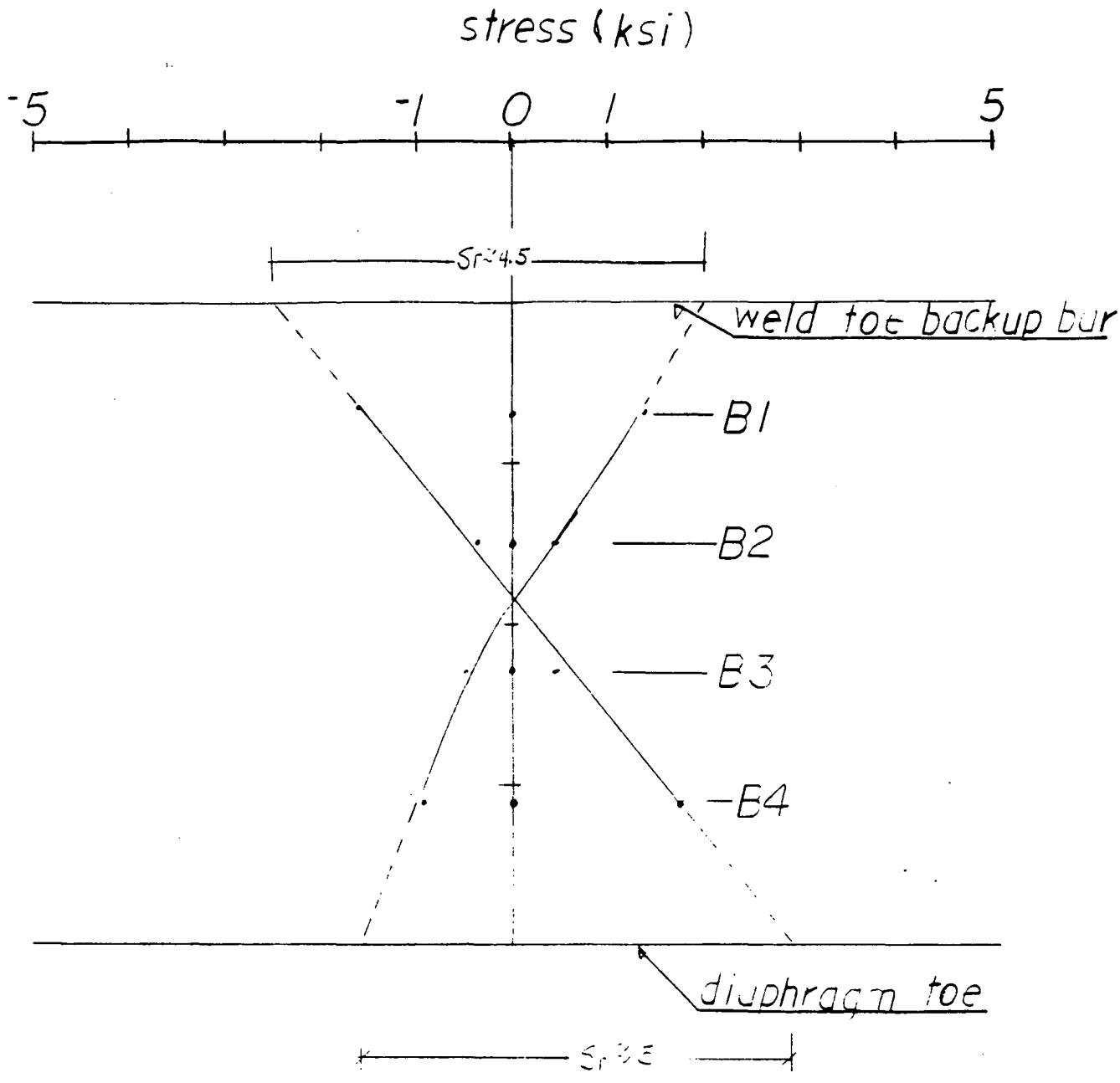

Fig. 49 Web Gap Stress Gradient in Region Adjacent to Top Flange - Outside Web Panel Point 4'

run #18

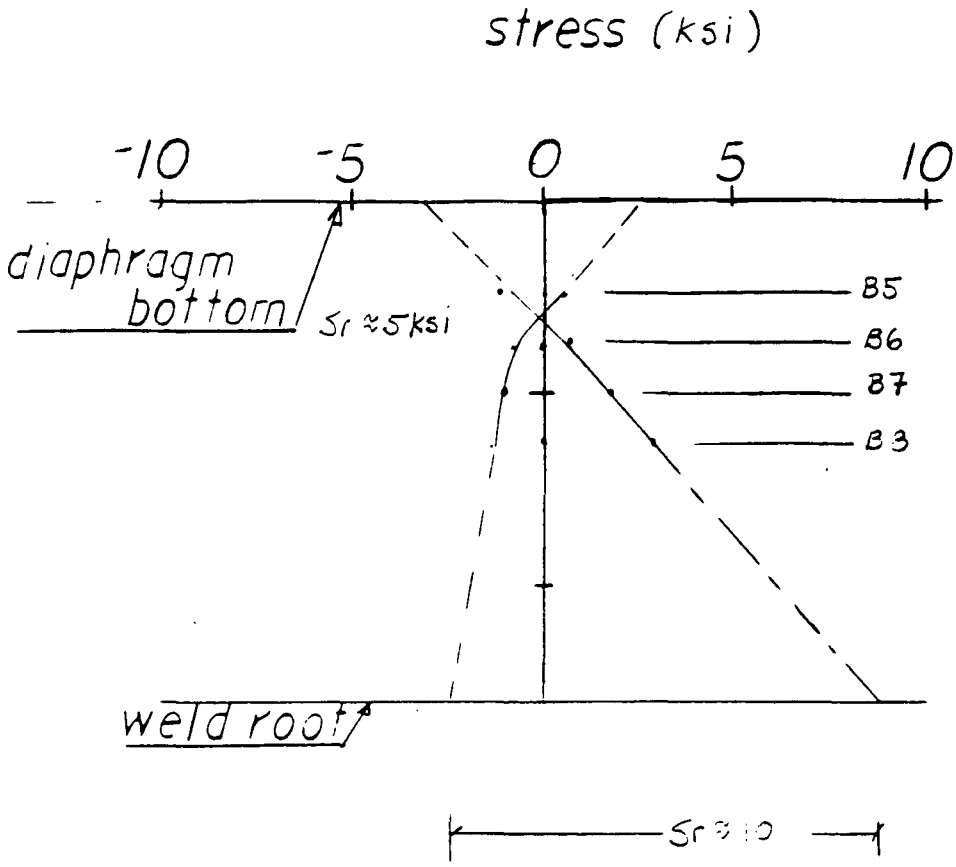

Fig. 50 Web Gap Stress Gradient in Region Adjacent to Bottom Flange - Outside Web Panel Point 4'

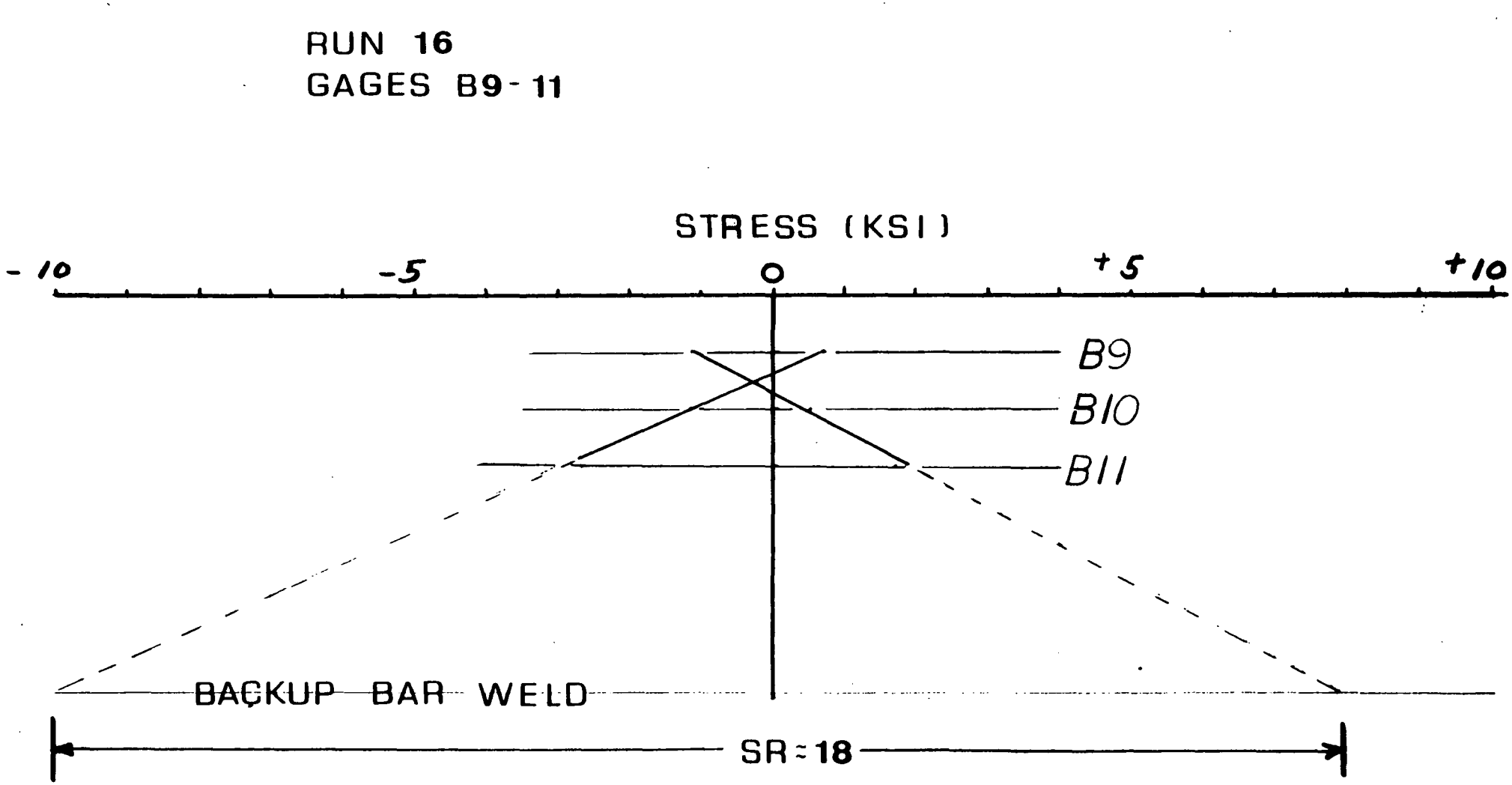

Fig. 51 Web Gap Stress Gradient in Region Adjacent to Bottom Flange - Inside Web of PP4', Run 16

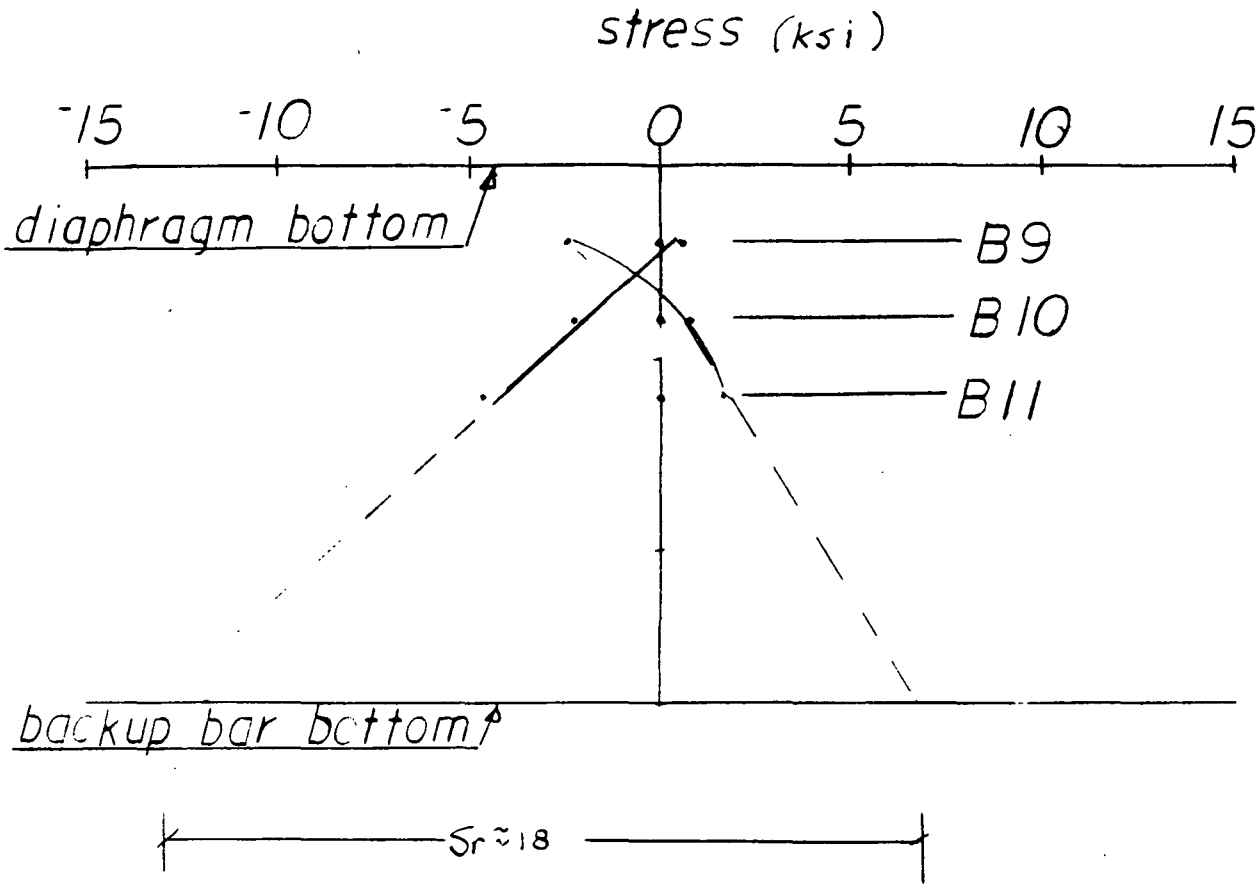

Fig. 52 Web Gap Stress Gradient in Region Adjacent to Bottom Flange - Inside Web Panel Point 4'

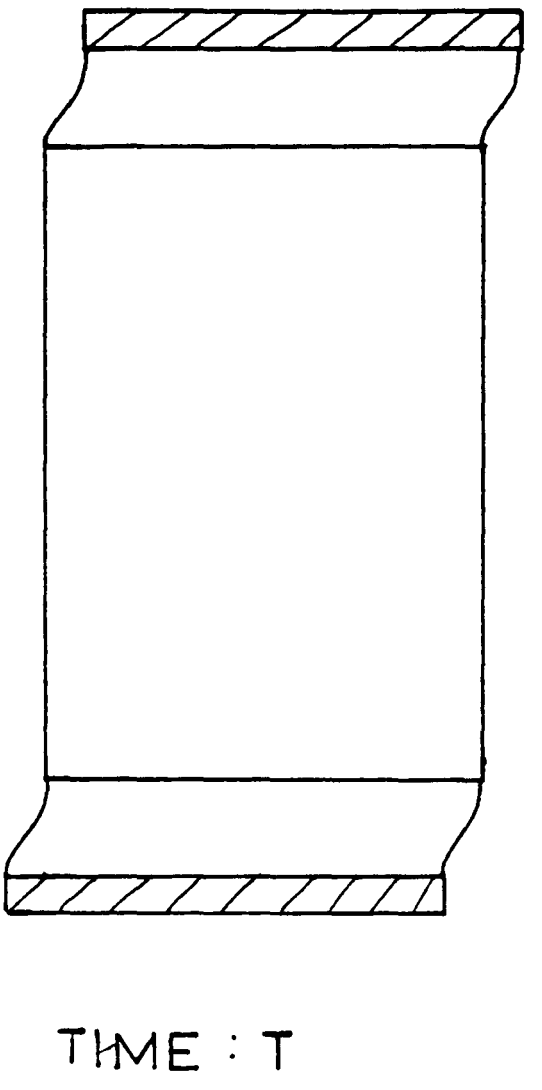

Fig. 53 Schematic of Distorted Cross-Section at Time T

RUN 18
B GAGES

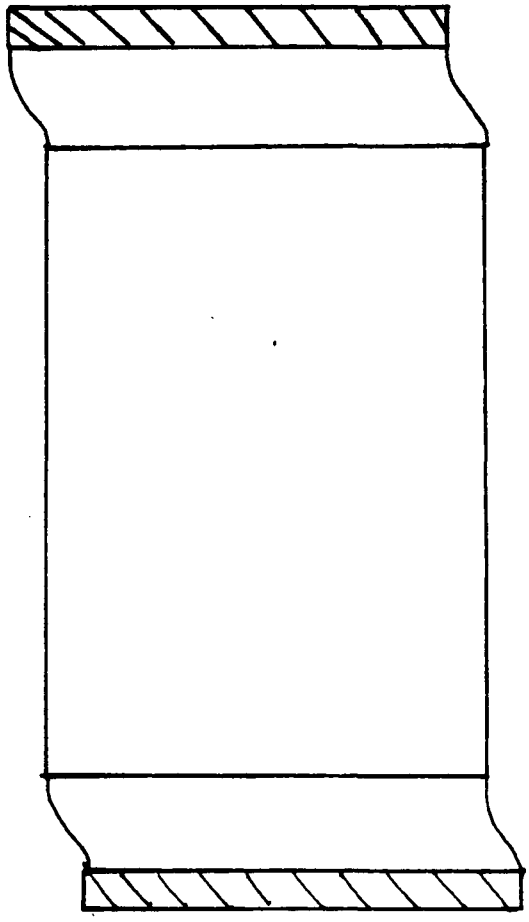

TIME : T+ t

Fig. 54 Schematic of Distorted Cross-Section at Time T + t

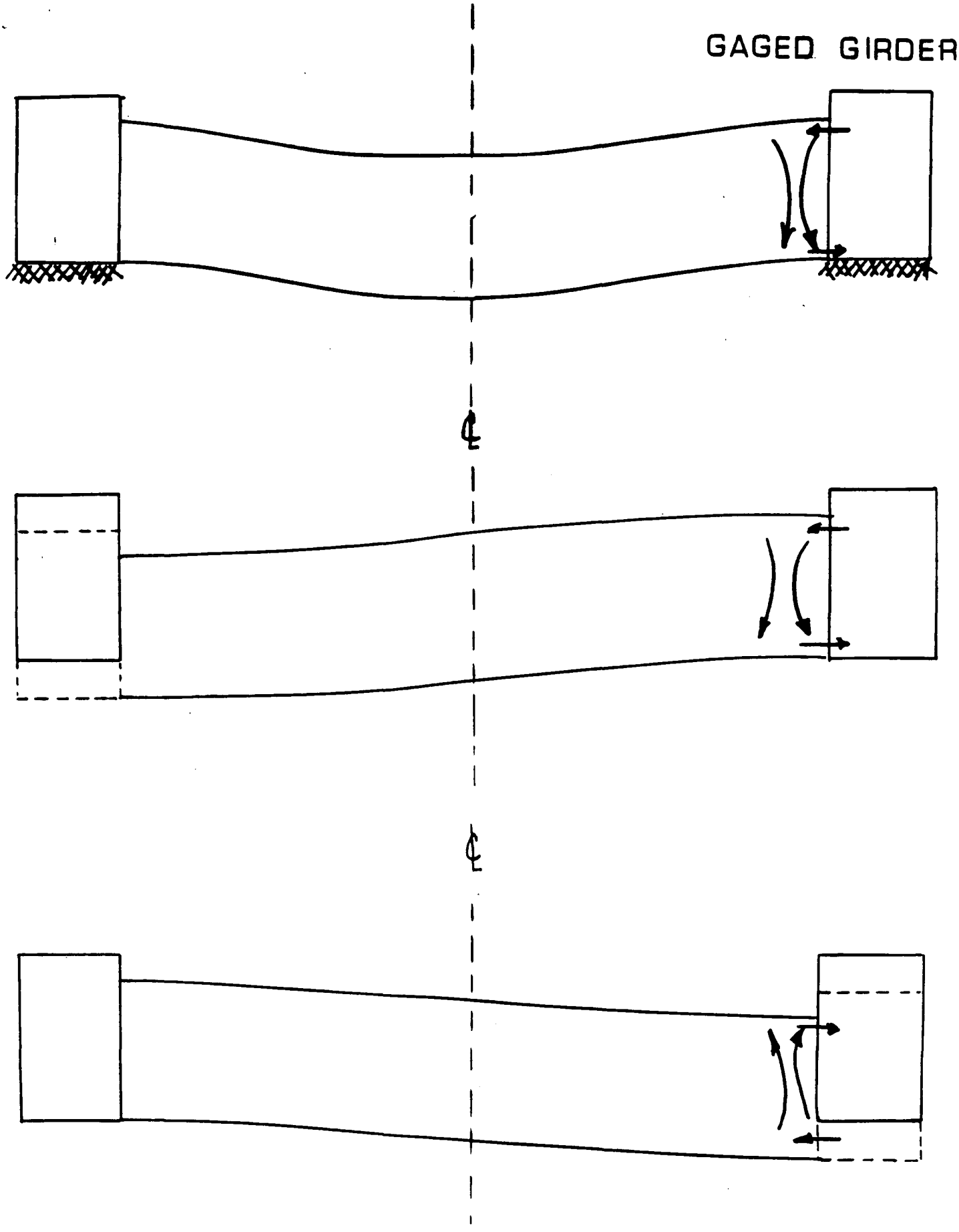

Fig. 55 Schematic Showing Possible Deformed Shapes of Floor Beam and Tie Girders

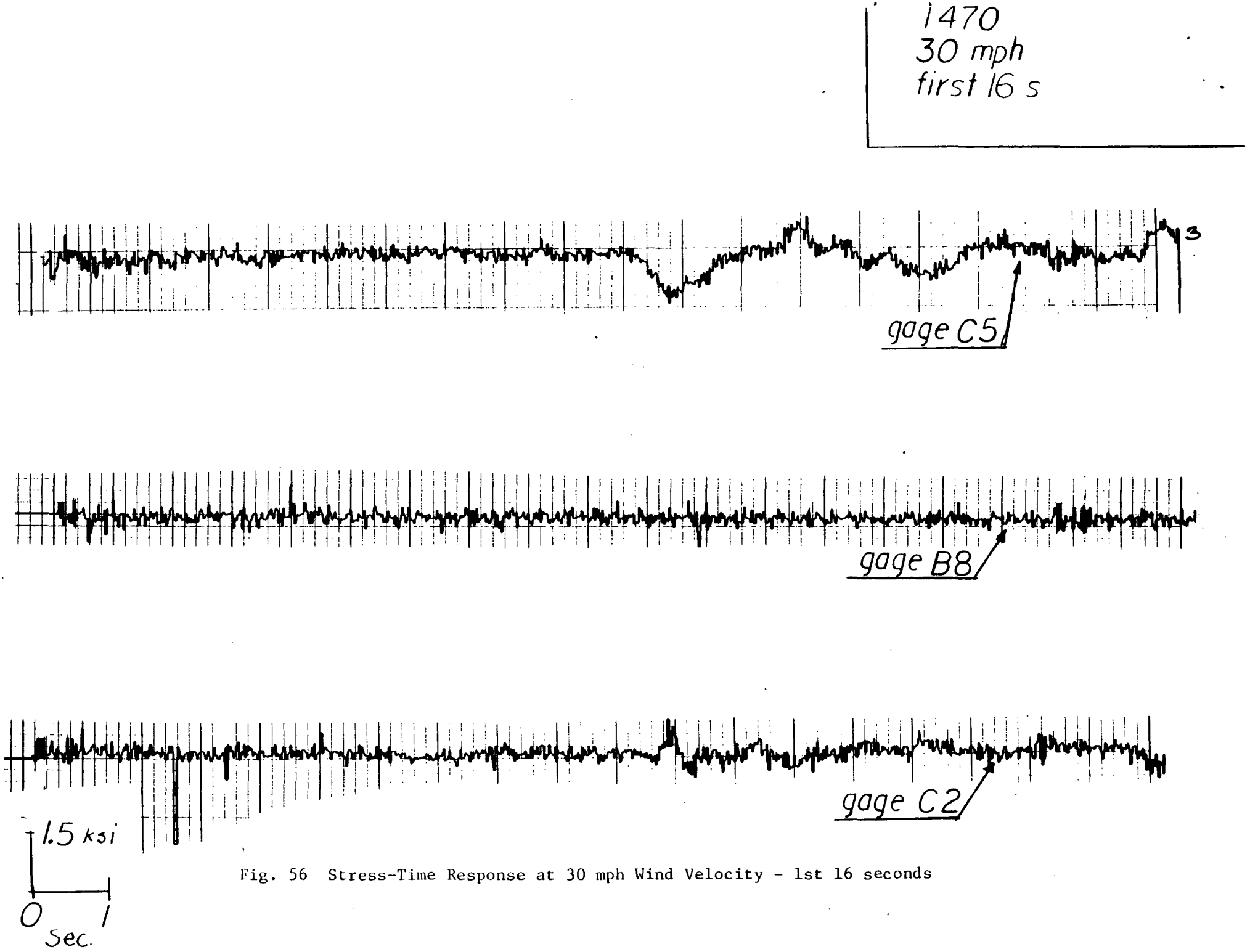

Fig. 56 Stress-Time Response at 30 mph Wind Velocity - 1st 16 seconds

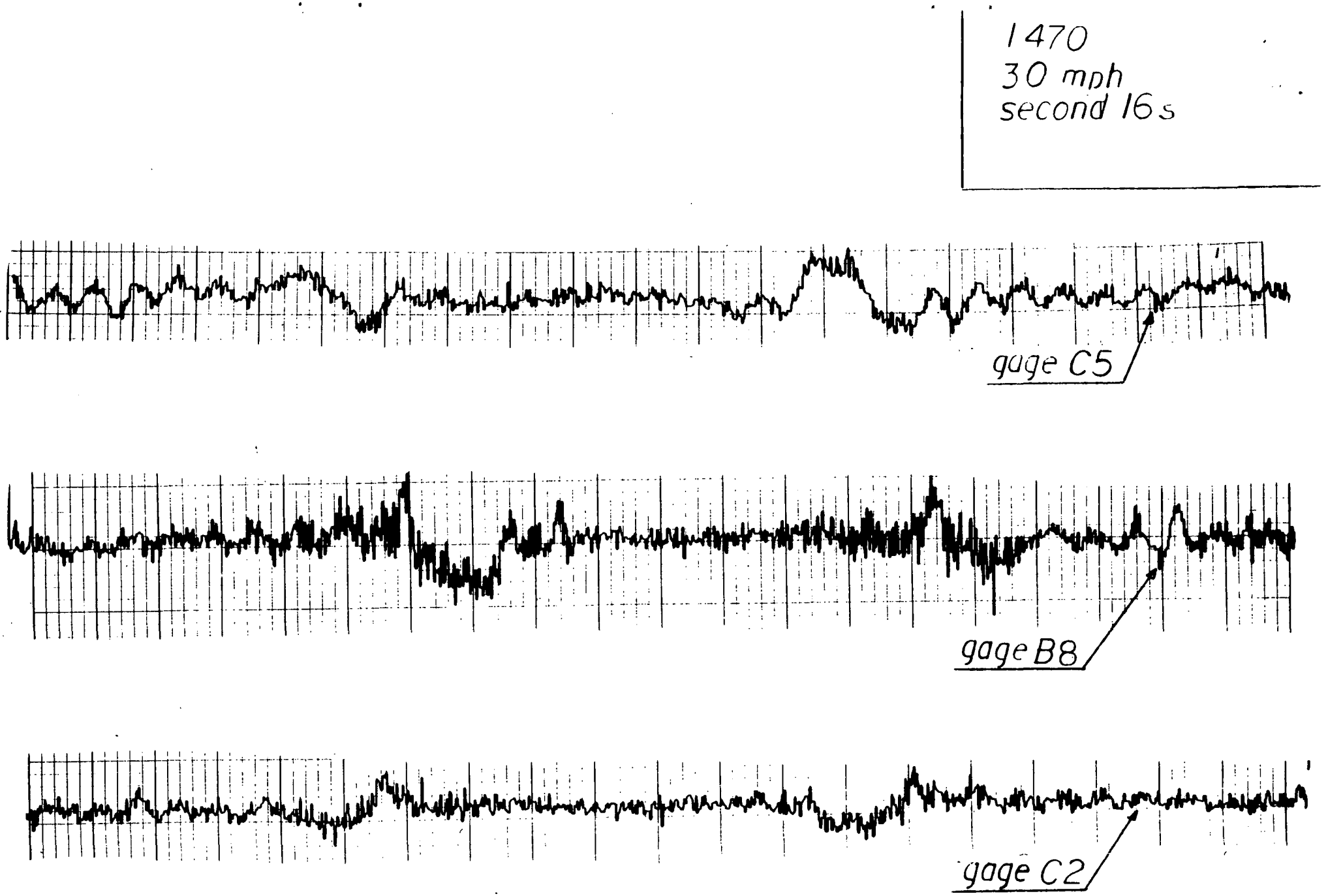

Fig. 57 Stress-Time Response at 30 mph Wind Velocity - 2nd 16 seconds

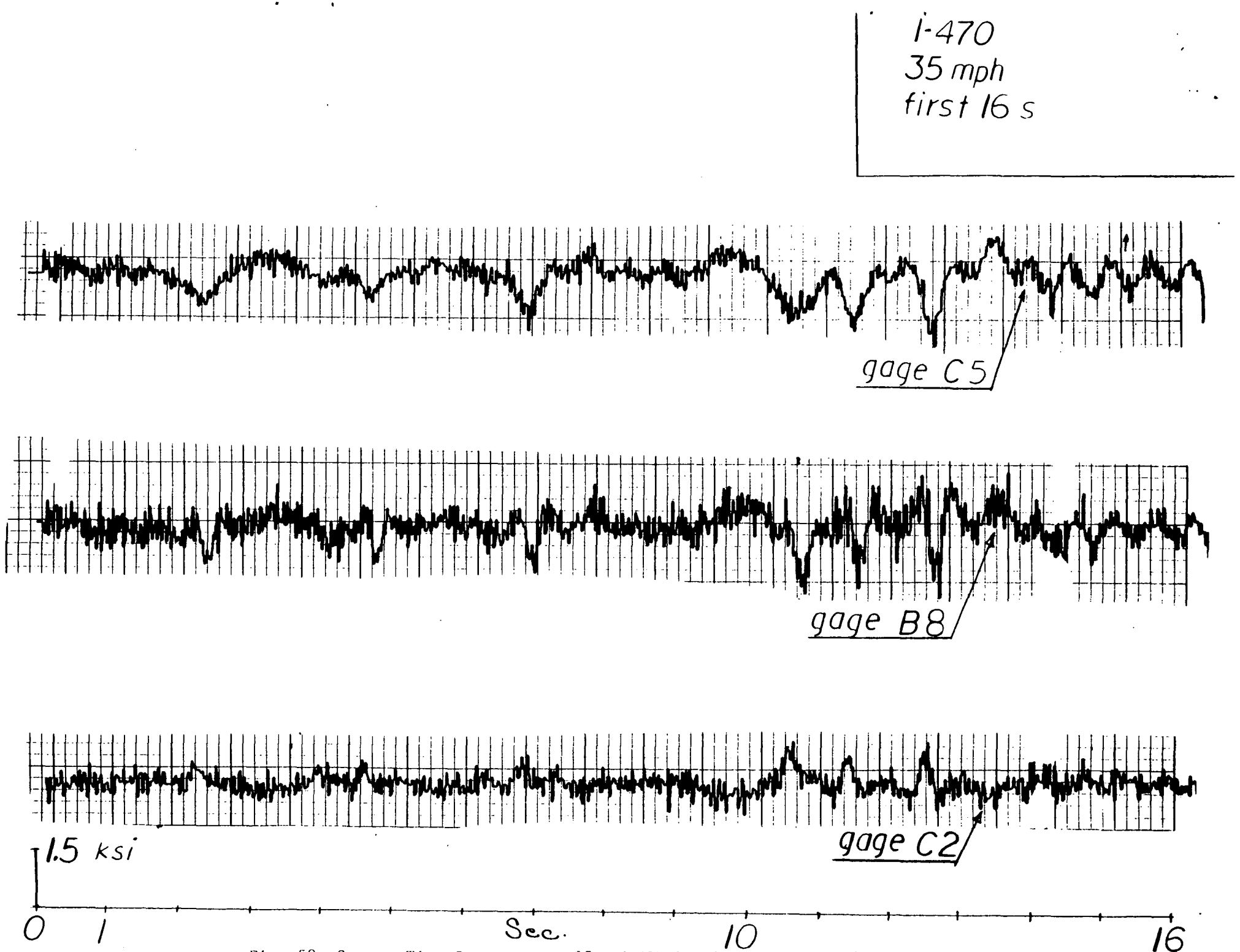

Fig. 58 Stress-Time Response at 35 mph Wind Velocity - 1st 16 seconds

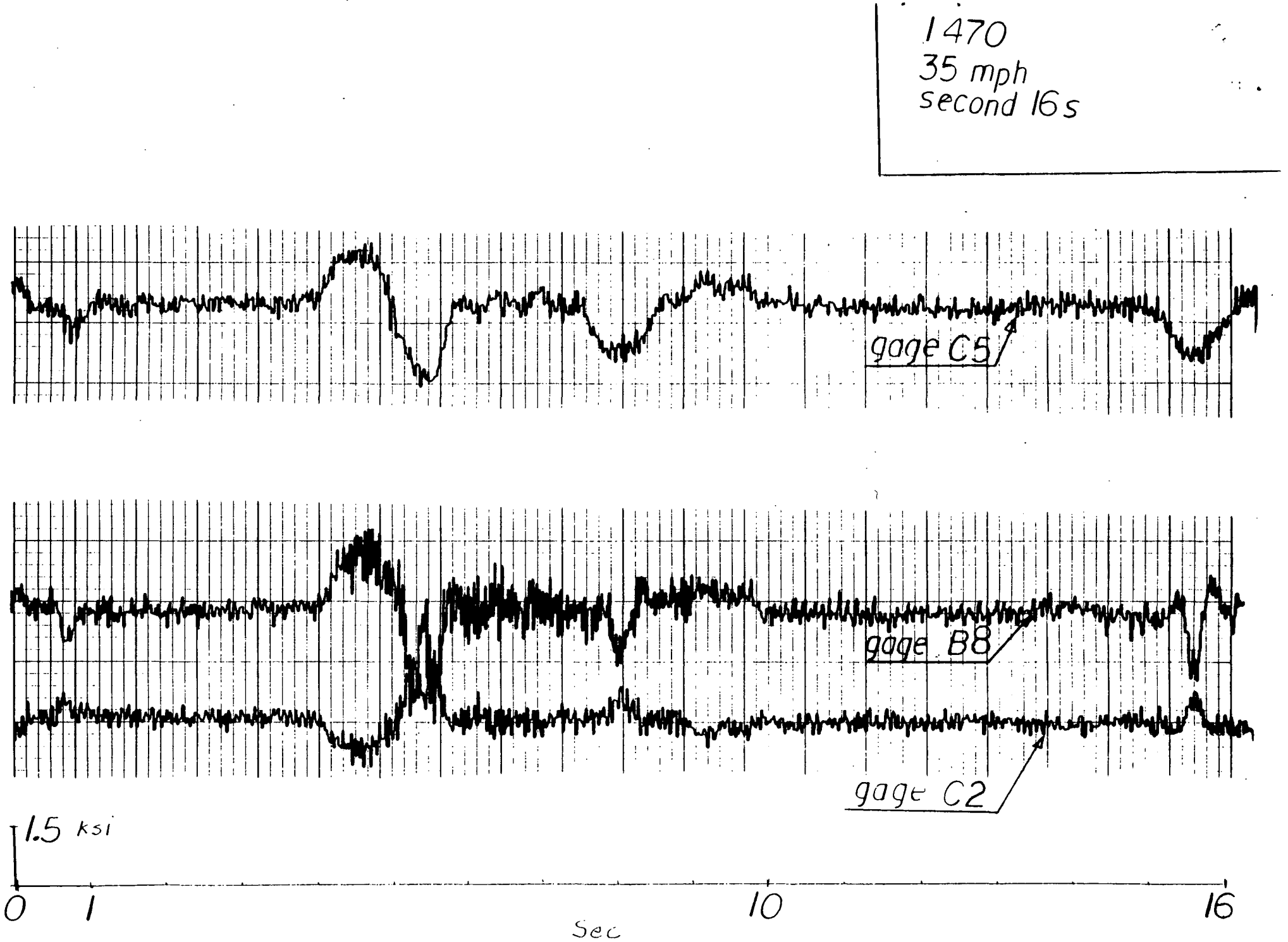

Fig. 59 Stress-Time Response at 35 mph Wind Velocity - 2nd 16 seconds

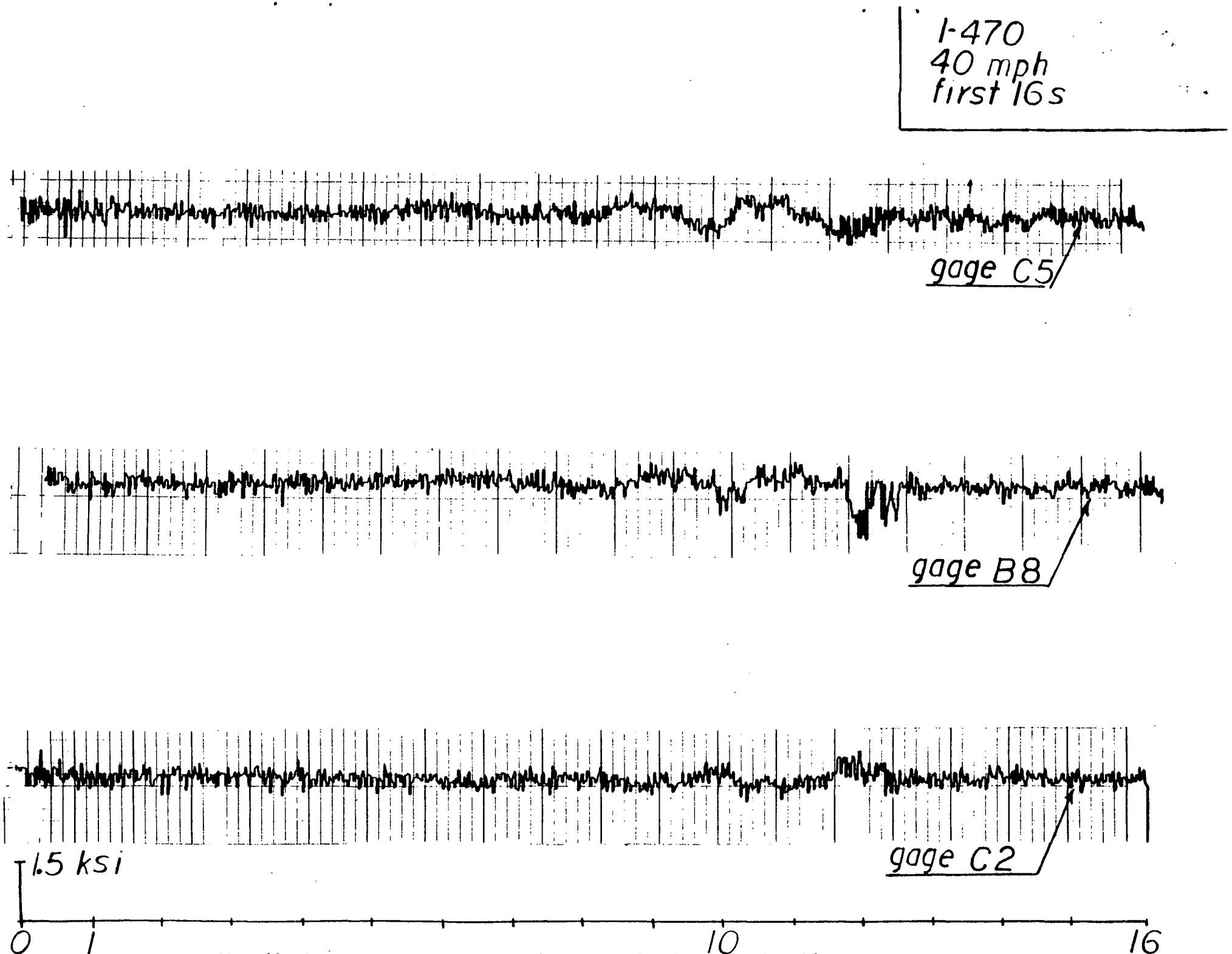

Fig. 60 Stress-Time Response at 40 mph Wind Velocity - 1st 16 seconds

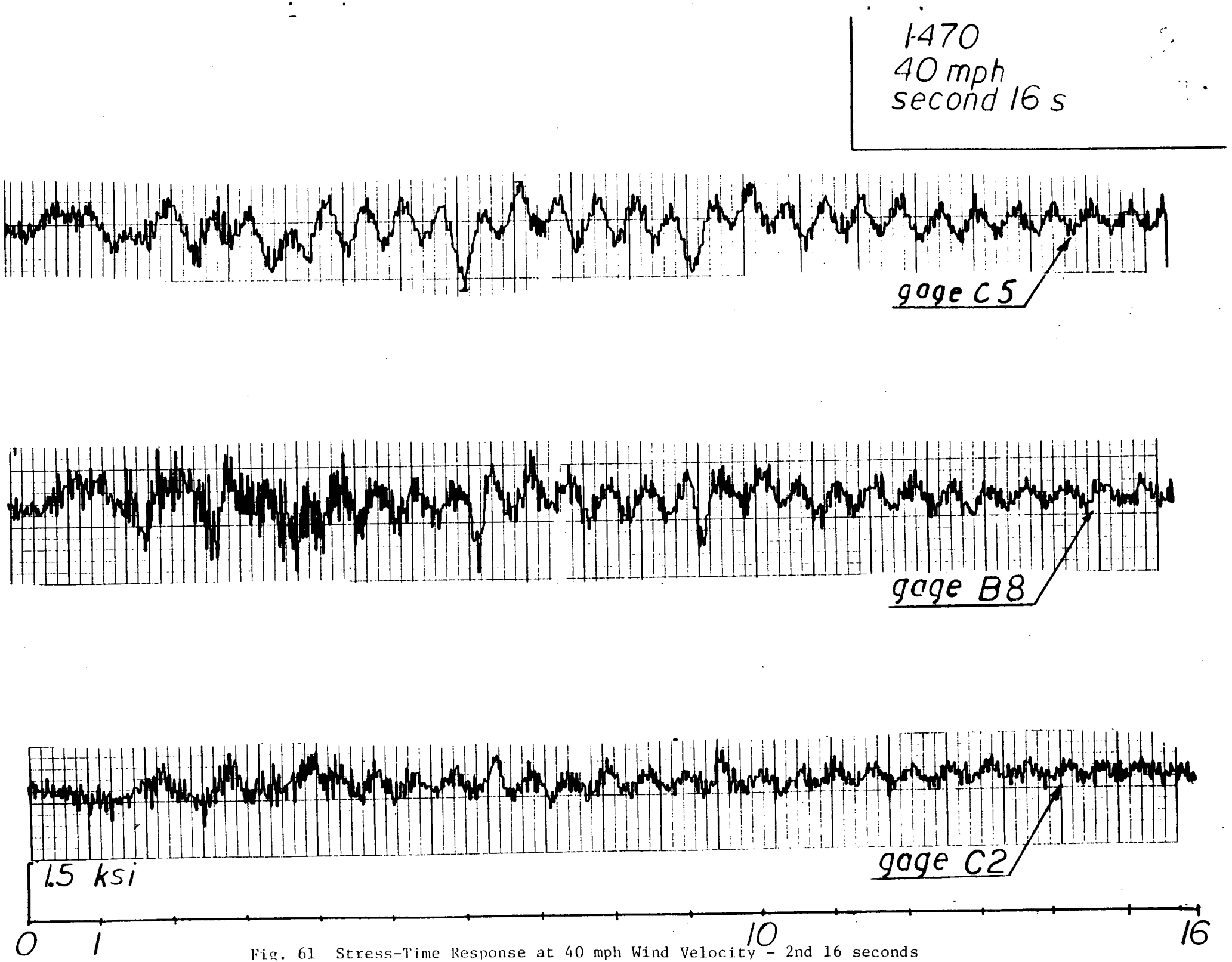

Fig. 61 Stress-Time Response at 40 mph Wind Velocity - 2nd 16 seconds

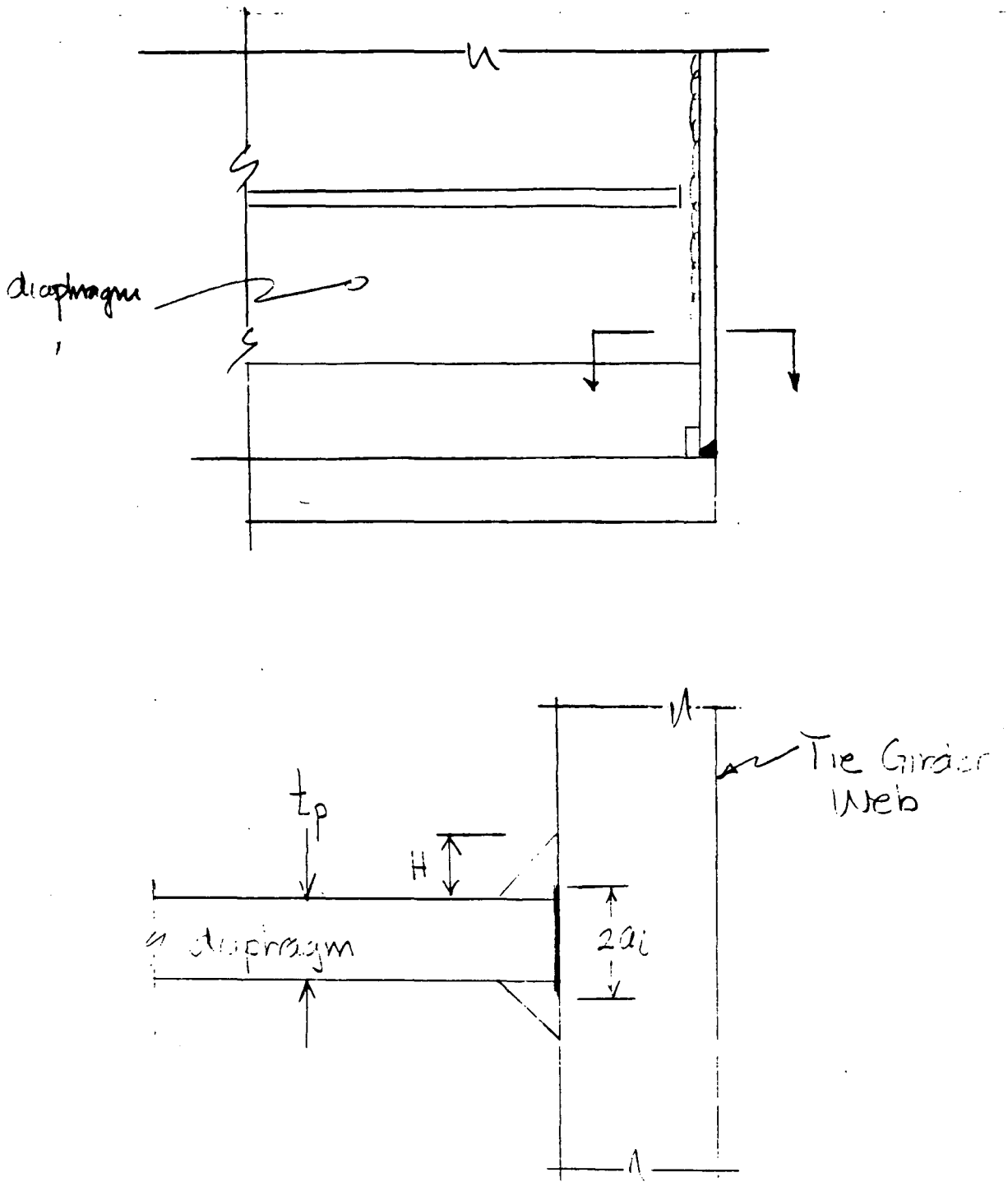

Fig. 62 Idealization for Crack Growth from the Fillet Weld Root

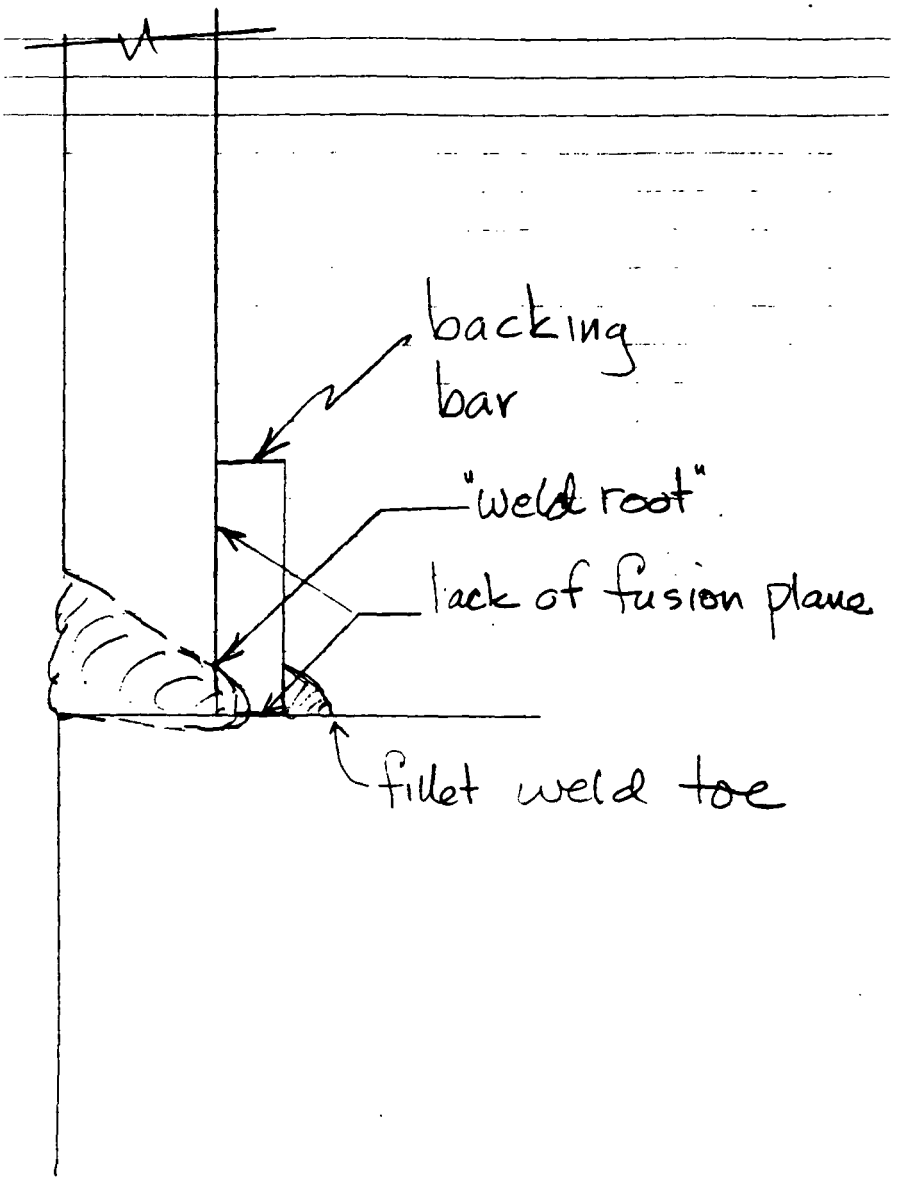

Fig. 63 Schematic of Box Corner Weld and Backing Bar Showing Lack of Fusion Planes

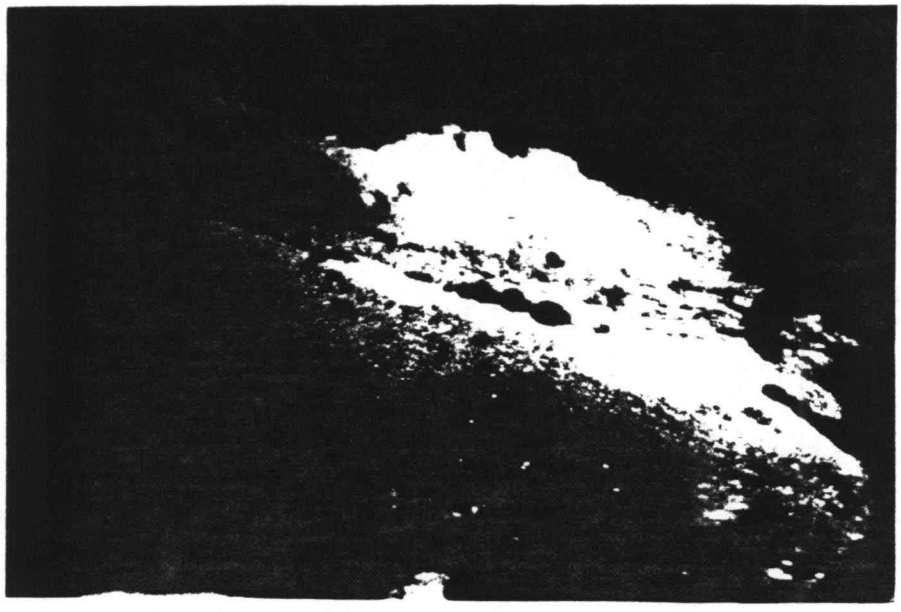

12/83/9-14

Fig. 64 Web Gap with Backing Bar Removed

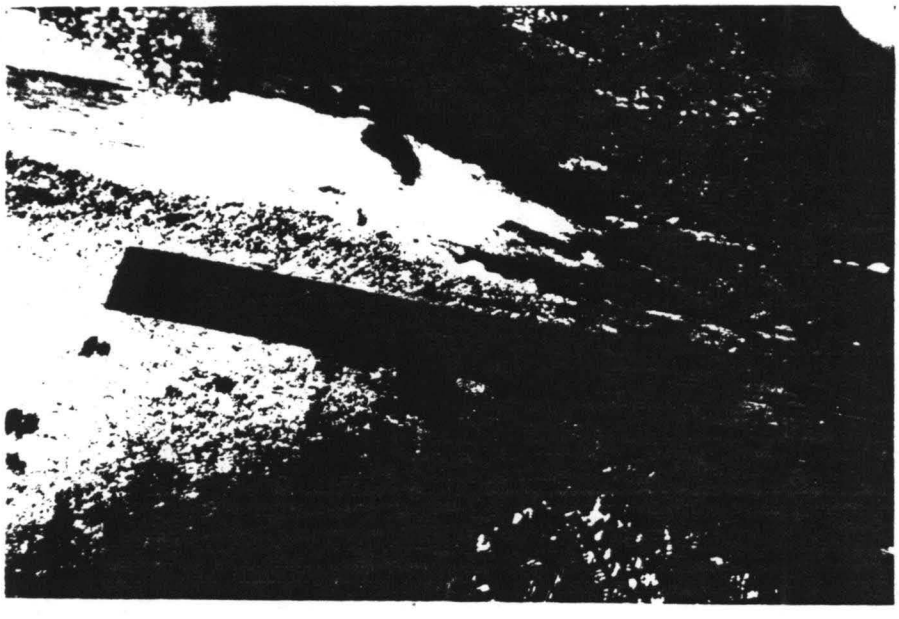

12/83/9-13

Fig. 65 Crack-like Indications Observed Where Fillet Weld Toe Existed Between Backing Bar and Flanges

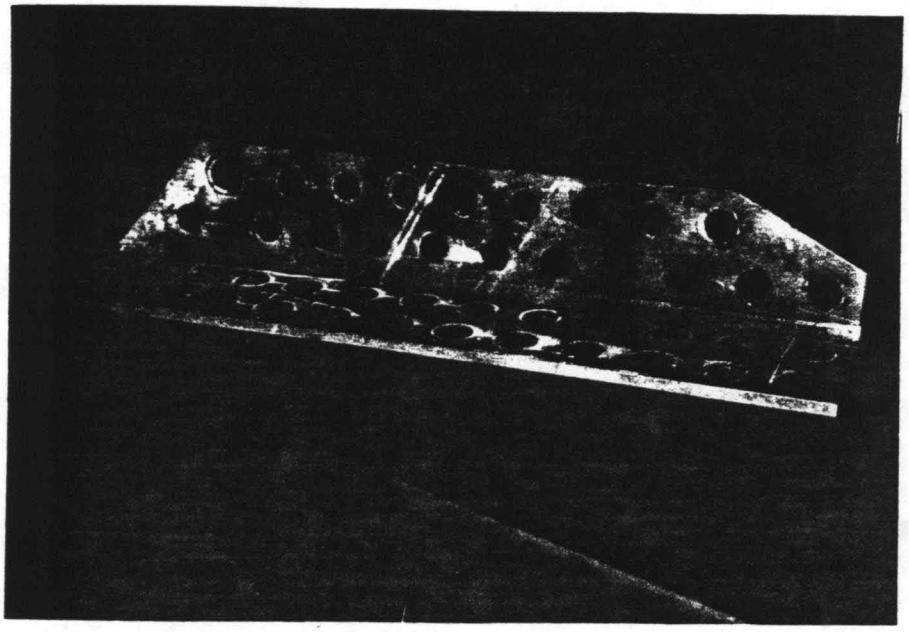

12/83/64-5

Fig. 66 Overall View of Cracked Hanger Support

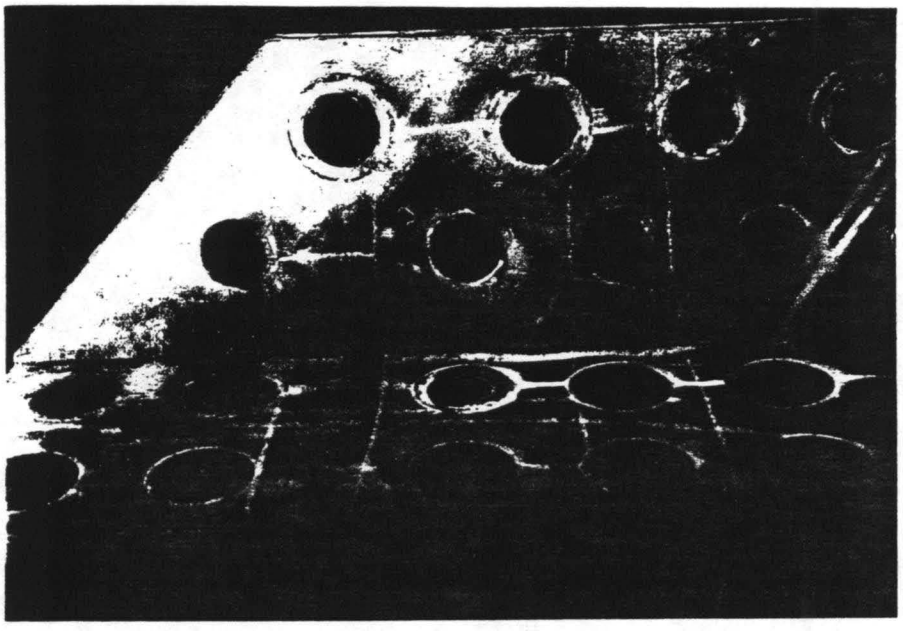

12/83/64-8

Fig. 67 Cracked Section (Left End)

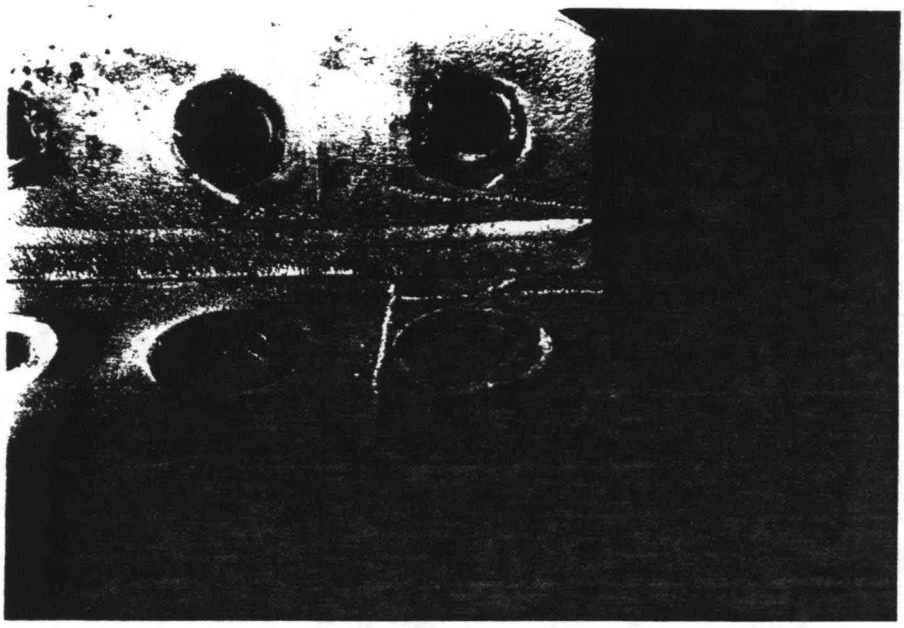

12/83/65-9

Fig. 68 Through Cracked Section (Right End)

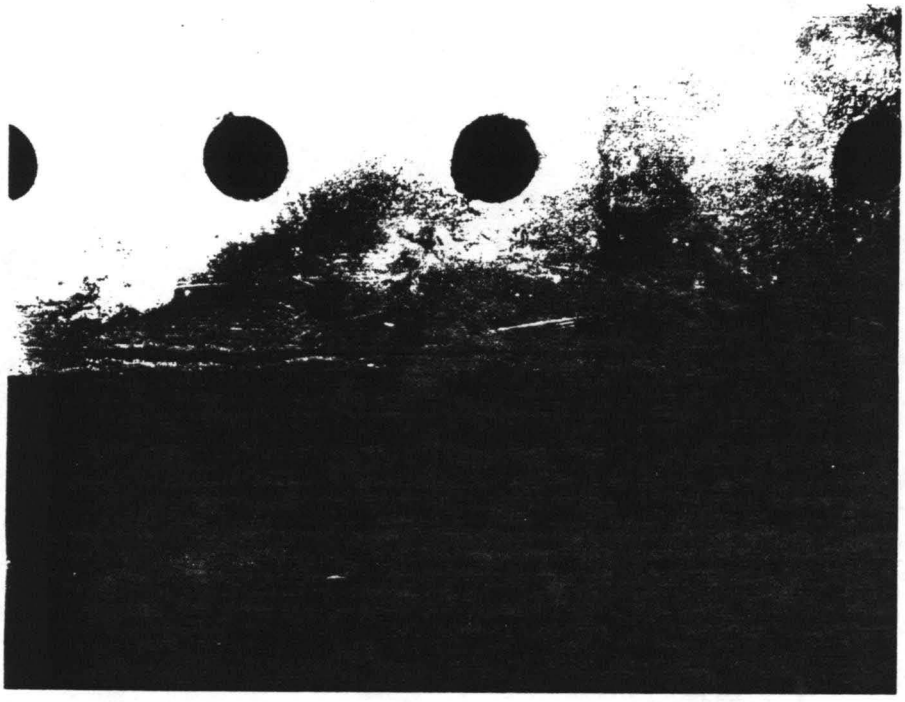

12/83/62-4

Fig. 69 Crack's Penetration on Outide of Angle

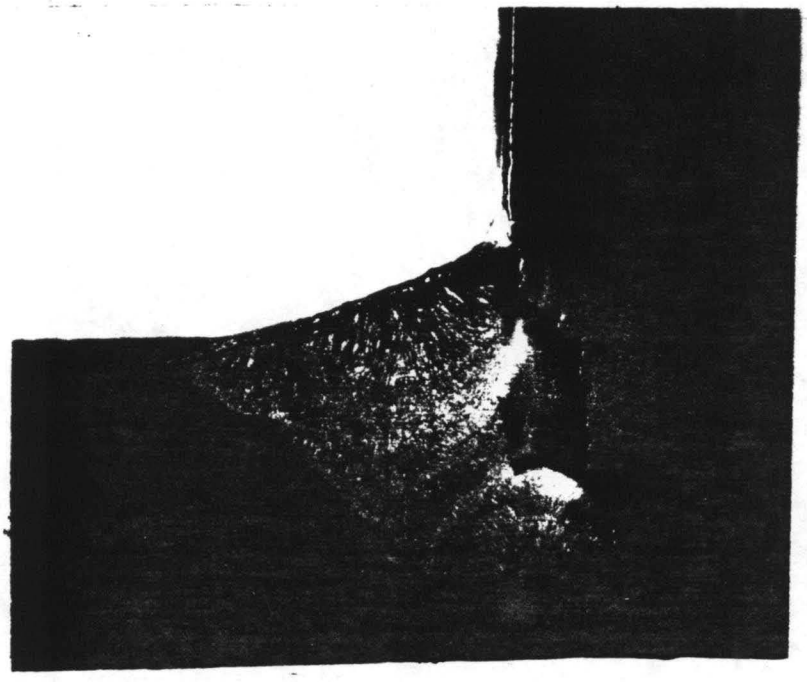

AWP

Fig. 70 Macroscopic Etched Section of Sample 1

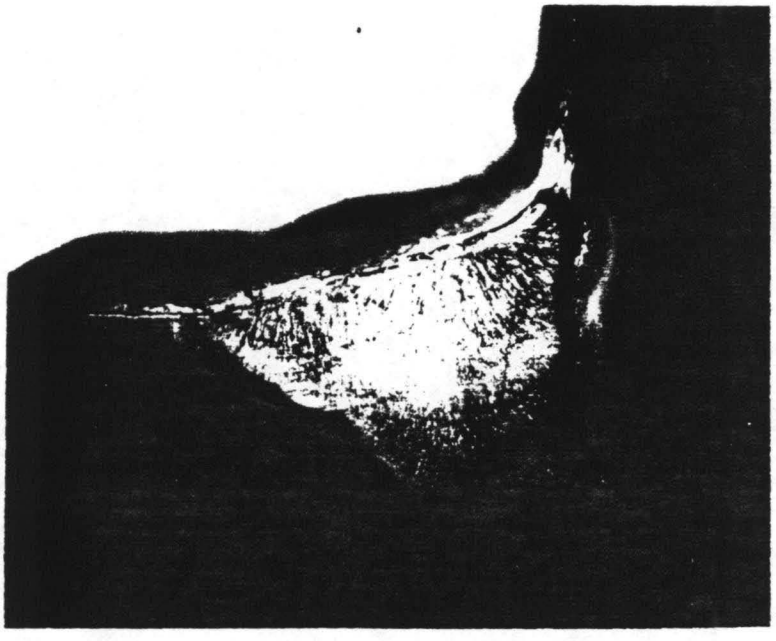

AWP

Fig. 71 Macroscopic Etched Section of Sample 2

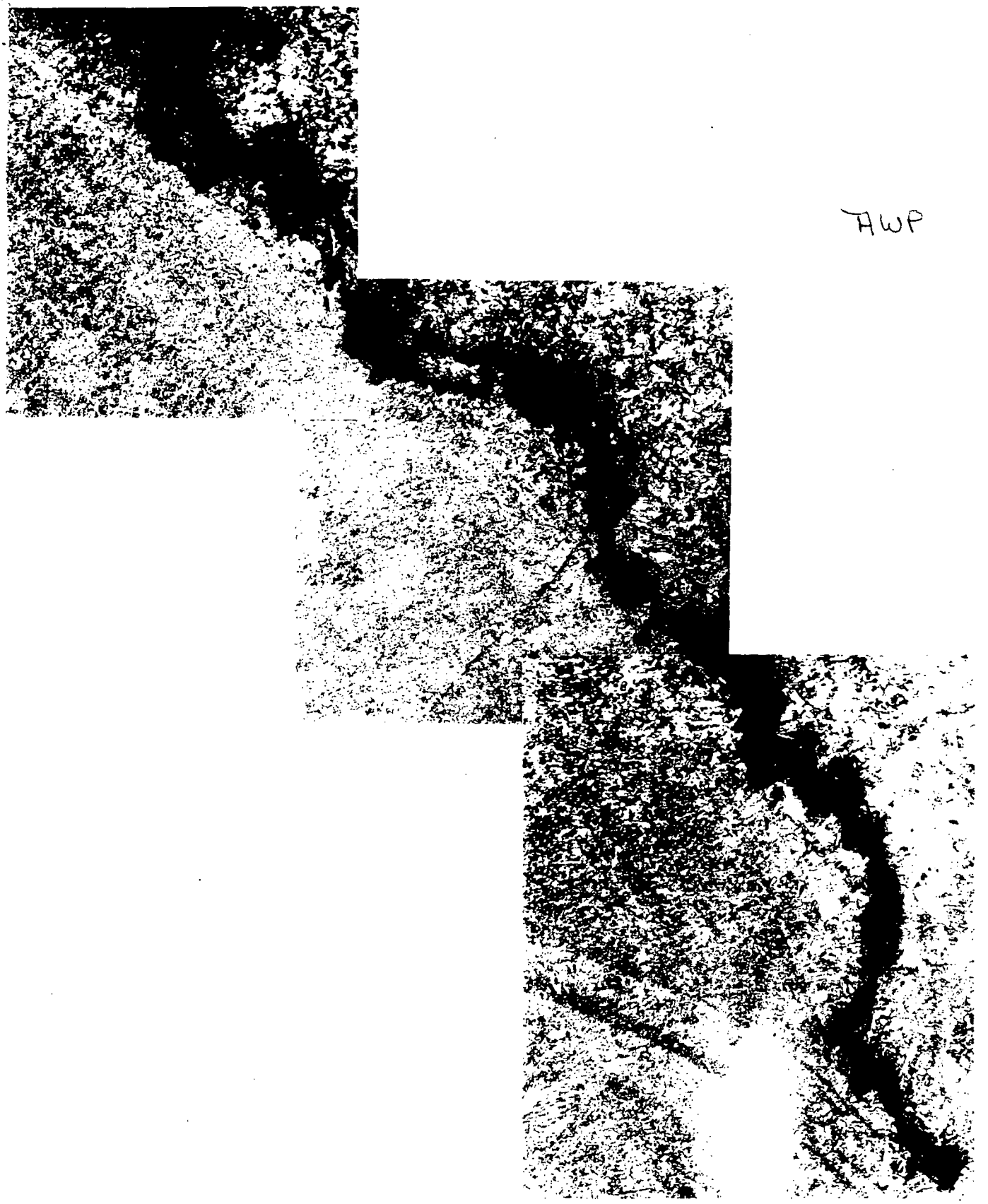

Fig. 72 Metallographic Section of Sample 1 (100X)

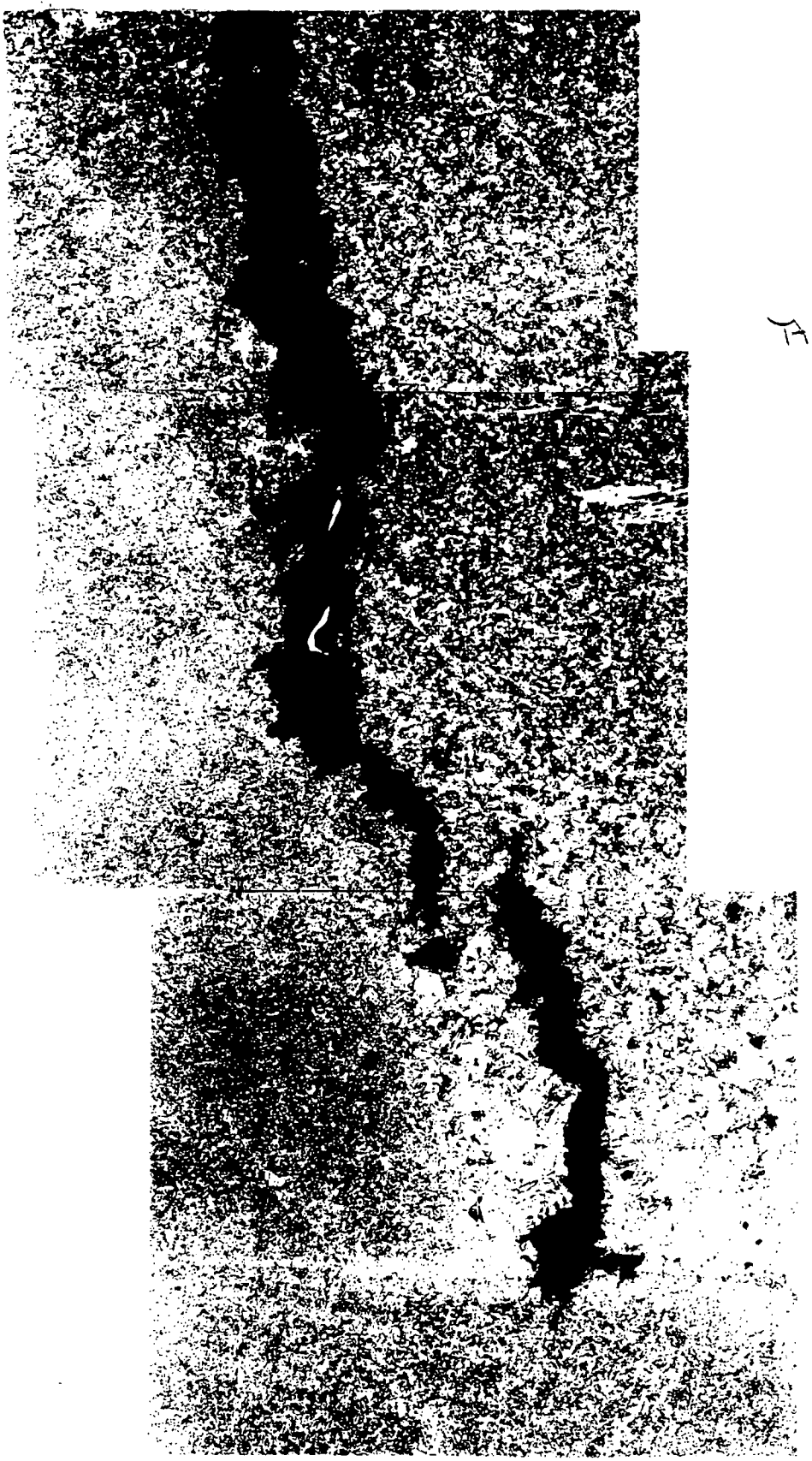

Fig. 73 Metallographic Section of Sample 2 (100X)

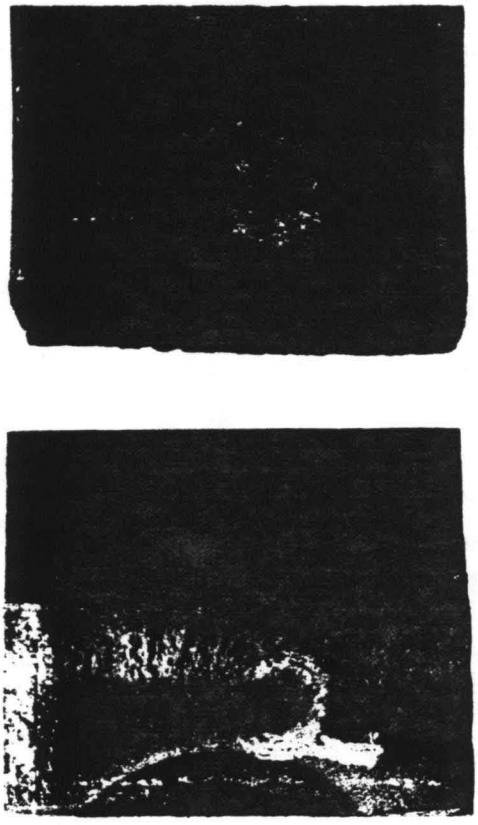

(a) Section Separated by Crack

(b) Paint Extending Beyond Weld Toe Onto Crack Surface

Fig. 74 Sawed Section Showing Exposed Crack Surfaces

Fig. 75 Crack Tip with Fatigue Extension, Sample 2 (100X)

REFERENCES

1. Frank, K. H. and Fisher, J. W.
FATIGUE STRENGTH OF FILLET WELDED CRUCIFORM JOINTS,
Journal of the Structural Division, ASCE, Vol. 105, ST9,
September 1979.

2. Vecchio, R. S. and Hertzburg, R. W.
AN EXAMINATION OF CLEANING TECHNIQUES FOR POST FAILURE ANALYSIS,
ASTM STP 827, 1983.

3. Modjeski and Masters, Consulting Engineers
Final Report, INVESTIGATION OF BROKEN WIRES IN SUSPENDER CABLES,
Bridge No. 2494, I470 over the Ohio River, October 1981.

4. Modjeski and Masters, Consulting Engineers
Finite Element Analysis Bridge N . 2494, I470 over the Ohio River
Proposed Tie Girder Retrofit, September 1984.

5. Kaufmann, E. J., Pense, A. W., and Stout, R. D.
AN EVALUATION OF FACTORS SIGNIFICANT TO LAMELLAR TEARING,
Welding Journal, Vol. 60, No. 3, March 1981, pp. 43s-49s.